



ARTICLE OPEN

A novel missense variant in ACAA1 contributes to early-onset Alzheimer's disease, impairs lysosomal function, and facilitates amyloid- β pathology and cognitive decline

Rongcan Luo¹✉, Yu Fan¹, Jing Yang^{1,2}, Maosen Ye^{1,2}, Deng-Feng Zhang¹, Kun Guo³, Xiao Li^{1,2}, Rui Bi¹, Min Xu¹, Lu-Xiu Yang¹, Yu Li^{1,2}, Xiaoqian Ran^{1,2}, Hong-Yan Jiang⁴, Chen Zhang⁵, Liwen Tan⁶, Nengyin Sheng^{3,7} and Yong-Gang Yao^{1,2,8}✉

Alzheimer's disease (AD) is characterized by progressive synaptic dysfunction, neuronal death, and brain atrophy, with amyloid- β (A β) plaque deposits and hyperphosphorylated tau neurofibrillary tangle accumulation in the brain tissue, which all lead to loss of cognitive function. Pathogenic mutations in the well-known AD causal genes including *APP*, *PSEN1*, and *PSEN2* impair a variety of pathways, including protein processing, axonal transport, and metabolic homeostasis. Here we identified a missense variant rs117916664 (c.896T>C, p.Asn299Ser [p.N299S]) of the acetyl-CoA acyltransferase 1 (*ACAA1*) gene in a Han Chinese AD family by whole-genome sequencing and validated its association with early-onset familial AD in an independent cohort. Further in vitro and in vivo evidence showed that *ACAA1* p.N299S contributes to AD by disturbing its enzymatic activity, impairing lysosomal function, and aggravating the A β pathology and neuronal loss, which finally caused cognitive impairment in a murine model. Our findings reveal a fundamental role of peroxisome-mediated lysosomal dysfunction in AD pathogenesis.

Signal Transduction and Targeted Therapy (2021)6:325

; <https://doi.org/10.1038/s41392-021-00748-4>**INTRODUCTION**

Alzheimer's disease (AD, MIM: 104300) is a devastating neurodegenerative disease that afflicts a large portion of the aged population at an ever increasing rate. Synaptic dysfunction, neuronal loss, amyloid plaques (main component amyloid- β (A β) peptide), tau inclusions (main component hyperphosphorylated tau), brain atrophy, and cognitive impairment are pathological and clinical features of AD.^{1,2} Accumulating evidence showed that both genetic and environmental factors affect AD, and its heritability has been estimated to be very high (up to 0.79).^{2–4} The genes involved in the A β production, such as *APP* (A β precursor protein), *PSEN1* (Presenilin-1), and *PSEN2* (Presenilin-2), were identified as the causal genes for some cases with early-onset familial AD (EOFAD) more than three decades ago.^{5–11} However, most of the pathogenic mutations of these causal genes presented in an autosomal-dominant manner and only occurred in a low proportion of (<5%) of AD patients.^{5,12} It has been shown that AD is polygenic, with many causal and/or risk genes remain to be identified.^{3,13–15} Over 40 well-confirmed AD risk loci have been reported in genome-wide association analyses (GWAS) of late-onset AD, with the APOE e4 allele being the most influential factor.^{13,14,16,17} Most of these GWAS loci are common single-nucleotide polymorphisms located in non-coding genomic

regions, with unknown function annotation and a small-to-moderate effect sizes (odds ratio [OR] <1.2). In fact, only 16% of the total AD phenotypic variance has been attributed to these GWAS hits,^{15,18} while other risk variants, especially these functionally causative variants^{14,15} in unknown genes and epigenetic alterations,^{19,20} still show some promise of helping our understanding of the complex genetic structure of AD. For instance, we recently found a missense variant p.K420Q in complement C7 to be associated with AD in Han Chinese.²¹

Over 50 loci/genes involved in a variety of pathways, including endocytosis, cholesterol and lipid metabolism, synaptic function, dendritic and axonal transport, A β and tau processing, and microglial and myeloid cell function, have been implicated in AD,^{14,22,23} suggesting that AD is a systemic disease.²⁴ There are multiple reports for dysfunction of metabolism during the AD pathogenesis.^{25–28} In this study, we reported an EOFAD-associated rare loss-of-function variant, rs117916664 (p.Asn299Ser [p.N299S]), in peroxisomal *ACAA1* (acetyl-CoA acyltransferase 1). The *ACAA1* p.N299S results in loss of function of the *ACAA1* enzyme and impairs the lysosomal function, disturbs global gene expression pattern, affects cellular function, and controls the expression network in human AD. Overexpression of *ACAA1* p.N299S in an AD mouse model facilitates A β pathology and exacerbates neurodegeneration.

¹Key Laboratory of Animal Models and Human Disease Mechanisms of the Chinese Academy of Sciences & Yunnan Province, and KIZ-CUHK Joint Laboratory of Bioresources and Molecular Research in Common Diseases, Kunming Institute of Zoology, Chinese Academy of Sciences, Kunming, Yunnan, China; ²Kunming College of Life Science, University of Chinese Academy of Sciences, Kunming, Yunnan, China; ³State Key Laboratory of Genetic Resources and Evolution, Kunming Institute of Zoology, Chinese Academy of Sciences, Kunming, China; ⁴Department of Psychiatry, The First Affiliated Hospital of Kunming Medical University, Kunming, China; ⁵Division of Mood Disorders, Shanghai Mental Health Center, Shanghai Jiao Tong University School of Medicine, Shanghai, China; ⁶Mental Health Institute of the Second Xiangya Hospital, Central South University, Changsha, China; ⁷Center for Excellence in Animal Evolution and Genetics, Chinese Academy of Sciences, Kunming, Yunnan, China and ⁸CAS Center for Excellence in Brain Science and Intelligence Technology, Chinese Academy of Sciences, Shanghai, China

Correspondence: Rongcan Luo (luorongcan@mail.kiz.ac.cn) or Yong-Gang Yao (yaoyg@mail.kiz.ac.cn)

These authors contributed equally: Rongcan Luo, Yu Fan.

Received: 5 May 2021 Revised: 13 August 2021 Accepted: 18 August 2021

Published online: 31 August 2021

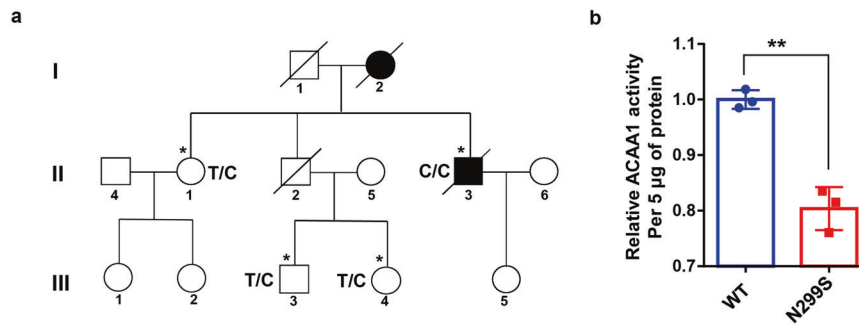


Fig. 1 The *ACAA1* c.896T>C (p.N299S) variant identified in a Han Chinese pedigree with familial AD disturbed acyltransferase activity. **a** Pedigree of a Han Chinese family with AD. Individuals who underwent whole-genome sequencing are indicated by asterisks (*). The subject with heterozygous or homozygous allele of rs117916664 was marked by T/C or C/C in the pedigree. **b** *ACAA1* p.N299S protein (N299S) has reduced enzyme activity compared to the wild-type *ACAA1* (WT). Purified *ACAA1* p.N299S and *ACAA1* WT were used for detection of acetyltransferase activity, with *ACAA1* WT as the reference ($n = 3$ biological replicates for each group). Results are mean \pm SD. ****** $P < 0.01$, Student's t test

Our results demonstrate that *ACAA1* p.N299S significantly aggravates A β pathologies and A β -mediated neurodegeneration, supporting a role of loss of function of *ACAA1* as a risk factor for AD development.

RESULTS

Association of *ACAA1* p.N299S with EOFAD in Han Chinese

We enrolled an EOFAD pedigree in Han Chinese from Southwest China (Fig. 1a) and performed whole-genome sequencing (WGS) on samples from four individuals in this family: the proband (II:3, male, 57 years) and his mother (I:2, female) had AD, but his sister (II:1, 63 years), one nephew (III:3, 34 years), and one niece (III:4, 27 years) were non-AD. No pathogenic mutations (rare damaging variants) in the three AD-causal genes *APP*, *PSEN1*, and *PSEN2* or other neurodegenerative disorder-causal genes were observed in the AD proband or in other individuals of this family (Supplementary Table S1). As there might be novel pathogenic mutation(s) accounting for the onset of EOFAD in this pedigree, we looked for rare (with a minor allele frequency [MAF] ≤ 0.01 in the dataset of the 1000 Genomes Project²⁹) and potentially damaging variants (including missense, nonsense, and frameshift variants). We identified a total of 58 rare potentially damaging variants and APOE $\epsilon 4$ in the four individuals (Supplementary Table S2). The three non-AD family members had the APOE $\epsilon 4$ allele, but the AD proband was APOE $\epsilon 4$ negative and had nine potentially damaging variants (*ACAA1* p.N299S, TET2 p.E1151*, TBC1D3D p.K25*, PSG4 p.Y351*, OR4X2 p.Y27*, SLC6A18 p.Y319*, GEMIN8 p.E195V, DMD p.K1510R, and GPR112 p.P368H); each variant had a genotype different from that of other non-AD members (Supplementary Table S2).

In order to investigate which variant might be associated with EOFAD, we screened for these 58 potentially damaging variants in the whole-exome sequencing data of 169 patients with EOFAD that were reported in our previous studies.^{21,30} The *ACAA1* variant (GenBank: NM_001130410.1: c.896T>C, rs117916664, p.N299S; PHRED-scaled Combined Annotation-Dependent Depletion (CADD) score³¹ 19.72), which was homozygous in the AD proband (Fig. 1a), was significantly enriched in EOFAD patients (MAF = 0.0525) compared to controls (MAF = 0.0204) (OR = 2.662, P value = 9.85×10^{-3}). The other eight damaging variants were either absent in the exome data^{21,30} or showed no association with AD (Supplementary Table S2). Note that, in European populations,^{32,33} variant *ACAA1* p.N299S has been shown to be extremely rare (MAF < 0.01%), indicating a population-specific effect.

Variant p.N299S impaired enzymatic activity of *ACAA1*

The *ACAA1* is named as peroxisomal 3-oxoacyl-coenzyme A thiolase or 3-ketoacyl-CoA thiolase, peroxisomal. Mutation

p.N299S occurs in an evolutionarily conserved residue in *ACAA1* (Supplementary Fig. S1). As *ACAA1* is a member of the acetyl-CoA acyltransferase family and plays an important role in fatty acid β -oxidation of the very-long-chain fatty acid (VLCFA),³⁴ we compared the enzymatic activities of wild-type (WT) *ACAA1* and mutant p.N299S by an in vitro enzymatic activity assay.³⁵ The enzymatic activity of *ACAA1* p.N299S is lower than that of *ACAA1* WT protein (Fig. 1b), indicating that *ACAA1* p.N299S is a loss-of-function variant causing a reduction in enzymatic activity.

ACAA1 p.N299S disturbed lysosomal and synaptic function

In order to gain an understanding of the biological consequences underlying the dysfunction of *ACAA1* enzyme at the molecular and cellular levels, we performed cellular assays using the U251 glioma cell line and the human microglia (HM) cell line overexpressing *ACAA1* WT and p.N299S, respectively. The U251 cells were of astrocyte origin and engineered to consistently express mutant APP p.K670N/M671L (U251-APP) and produced A β under doxorubicin induction in our previous studies.^{36,37} RNA sequencing (RNA-seq) analyses were performed for the HM and U251-APP cells overexpressed with empty vector, *ACAA1* WT, and *ACAA1* p.N299S, respectively. We observed a clear distinction between the *ACAA1* p.N299S and *ACAA1* WT groups and between the *ACAA1* p.N299S and the empty vector groups for both HM and U251-APP cells based on the principal component analysis (Supplementary Fig. S2a). The heatmap of the dysregulated genes in both cell lines also showed a significant difference between the *ACAA1* p.N299S and *ACAA1* WT groups (Supplementary Fig. S2b), indicating that the mutant p.N299S has an effect on the gene expression pattern. We identified 1219 differentially expressed genes (DEGs; $P_{\text{adjust}} < 0.05$) between the *ACAA1* p.N299S and *ACAA1* WT groups that were shared by both the HM and U251-APP cells, of which 734 genes were upregulated and 485 were downregulated (Supplementary Fig. S2c). According to Kyoto Encyclopedia of Genes and Genomes (KEGG) pathway³⁸ and Gene Ontology (GO) biological processes enrichment analyses,³⁹ these DEGs were enriched in processes involved in lysosomal activity, cellular senescence, axon guidance, synaptic plasticity, fatty acid oxidation, and cognition (FDR [false discovery rate] < 0.05, Fig. 2a and Supplementary Table S3). Gene Set Enrichment Analysis (GSEA)⁴⁰ indicated that these DEGs were strongly enriched in the GO terms "neurogenesis," "neuron development," and "neuron differentiation" (FDR < 1.00×10^{-6} , Figs. 2b and Supplementary Fig. S2d). KEGG pathway enrichment analysis of the U251-APP cells also showed that dysregulated genes in the *ACAA1* p.N299S group were significantly enriched in the AD pathway (hsa05010, FDR = 2.26×10^{-18} , Supplementary Table S3), consistent with the

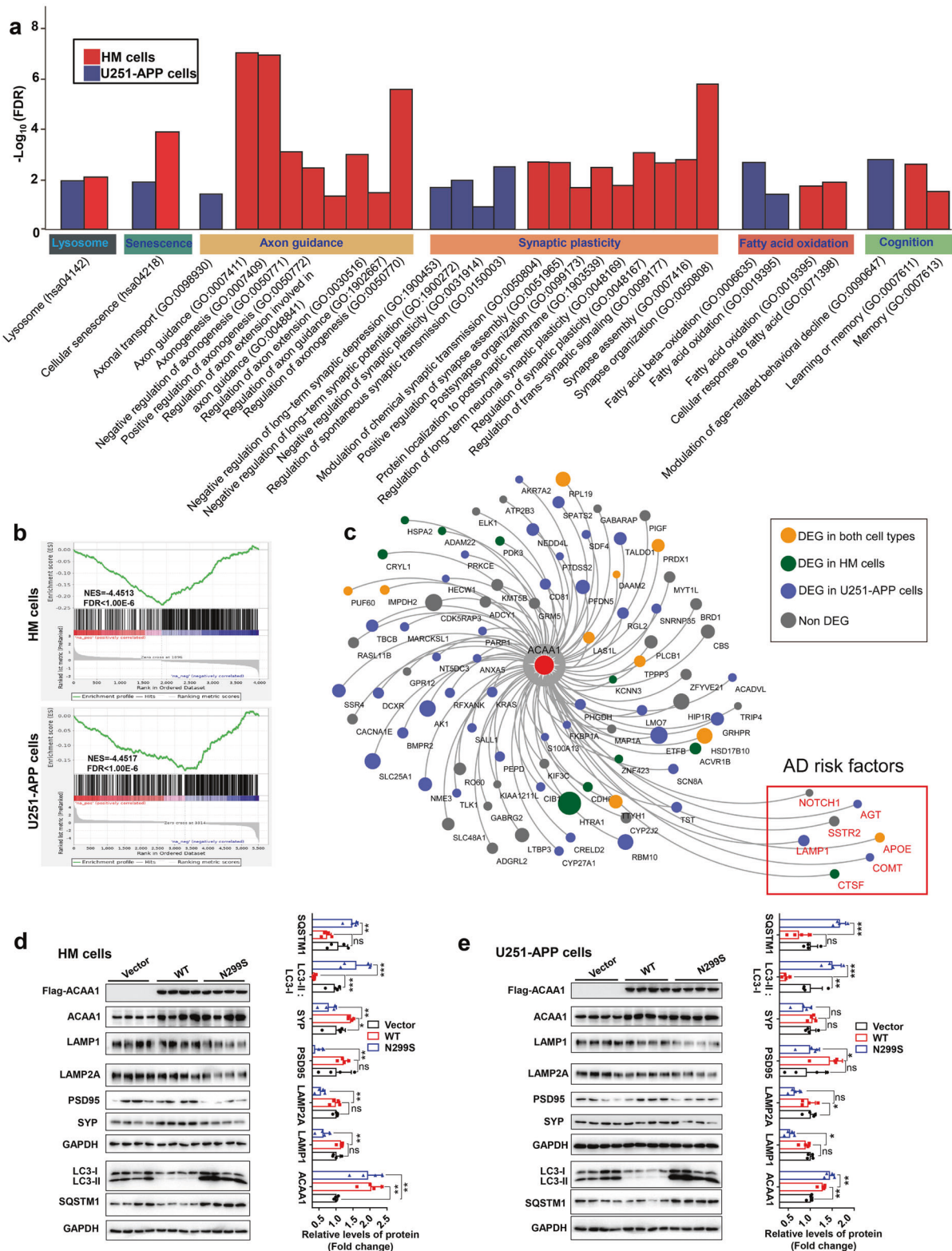


Fig. 2 Overexpression of ACAA1 p.N299S disturbed global gene expression pattern and inhibited lysosomal and synaptic proteins in human cells. **a** KEGG pathway and GO biological processes analyses of differentially expressed genes in the HM and U251-APP cells overexpressing ACAA1 p.N299S and ACAA1 WT. **b** Enrichment of neuron development genes in cells with overexpression of ACAA1 p.N299S versus ACAA1 WT (upper, HM cells; below, U251-APP cells) based on gene set enrichment analyses (GSEA). **c** Overexpression of ACAA1 p.N299S versus ACAA1 WT affects co-expression network constructed using human AD brain tissues. **d**, **e** Overexpression of ACAA1 p.N299S in HM (**d**) and U251-APP cells (**e**) reduced the levels of lysosomal and postsynaptic proteins and increased LC3-II:LC3-I ratio and SQSTM1 protein level. The GAPDH was used as the loading control. Data are representative of three independent experiments with similar results. Bars represent mean \pm SD of the three experiments. ns, not significant; * $P < 0.05$; ** $P < 0.01$; *** $P < 0.001$; Student's *t* test

background introduction of mutant APP p.K670N/M671L in this cell line.^{36,37}

The DEGs between ACAA1 p.N299S and ACAA1 WT were significantly enriched ($P < 0.05$, Fisher's exact test) in a co-expression network ($P_{\text{adjust}} < 0.0001$) (Fig. 2c) that was found to be abnormally regulated in brain tissues of AD patients,⁴¹ in which ACAA1 was located in a central position of the network. A group of genes associated with late-onset AD implicated in lipid metabolism (APOE [apolipoprotein E]),^{42,43} immune response (APOE, AGT [angiotensinogen]),⁴¹ and the lysosome pathway (CTSF [cathepsin F], LAMP1 [lysosomal associated membrane protein 1])⁴⁴ were involved in this network. COMT (catechol-O-methyltransferase), a previously reported AD gene,⁴⁵ was also dysregulated by ACAA1 p.N299S (Fig. 2c).

The lysosome-related pathologies, together with neuron loss and A β plaque deposition, have been shown to be accentuated in EOFAD due to mutations in PSEN1.⁴⁶ We tested the protein levels of lysosomal markers LAMP1 and LAMP2A (lysosomal-associated membrane protein 2), autophagy markers MAP1LC3/LC3 (microtubule-associated protein 1 light chain 3) and SQSTM1 (sequestosome 1), and synaptic markers DLG4/PSD95 (Discs large MAGUK scaffold protein 4) and SYP (synaptophysin) in cells overexpressing ACAA1 p.N299S compared to those of cells overexpressing ACAA1 WT. We found a significant decrease in the protein levels of LAMP1, LAMP2A, PSD95, and SYP and a significant increase in the levels of LC3-II:LC3-I ratio and SQSTM1 in cells overexpressing ACAA1 p.N299S, suggesting potential dysfunction of synaptic transmission and lysosomal function in HM cells (Fig. 2d) and U251-APP cells (Fig. 2e). To characterize the roles of ACAA1 in lysosomal and synaptic function, we generated ACAA1-deficient HM and U251-APP cells (ACAA1-KO) using the CRISPR/Cas9-mediated genome editing method (Supplementary Fig. S3a, b). Consistent with the overexpression effect of ACAA1 p.N299S (Fig. 2d, e), knockout (KO) of ACAA1 significantly impaired the lysosomal and synaptic protein expression, as characterized by the reduced protein levels of PSD95, SYP, LAMP1, LAMP2A, CTSD (cathepsin D), CTSD (cathepsin B), and TFEB (transcription factor EB) and the increased LC3-II:LC3-I ratio and SQSTM1 protein level in both ACAA1-deficient U251-APP (Supplementary Fig. S3c) and HM cells (Supplementary Fig. S3d). We repeated the above results in a neuronal cell line SH-SY5Y cells by using small interfering RNA (siRNA) knockdown assays. Three siRNAs were designed for ACAA1 and siRNA-1 (25 nM) was found to have the best inhibitory effect (Supplementary Fig. S4) and was used in the following assays. We confirmed that both ACAA1 knockdown and ACAA1 p.N299S overexpression impaired lysosomal and synaptic protein expression in SH-SY5Y cells (Supplementary Fig. S5). These data suggested that endogenous ACAA1 was critically involved in lysosomal and synaptic function, and ACAA1 p.N299S might impair lysosomal function and disturb synaptic function.

Virus-mediated overexpression of ACAA1 p.N299S exacerbated cognitive decline in APP/PS1 Δ E9 mice

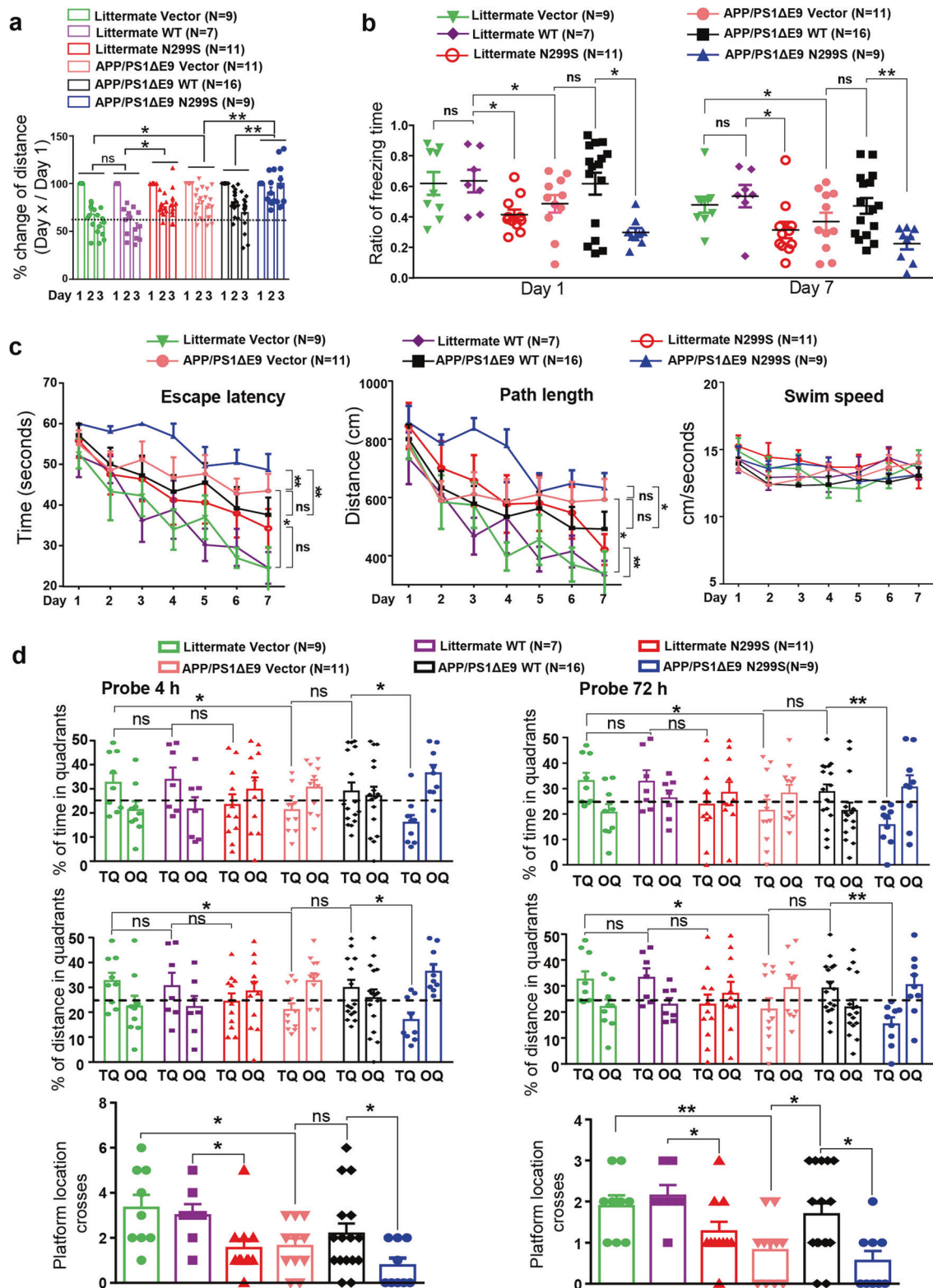
We investigated whether ACAA1 p.N299S would play a vital role in AD pathogenesis by using the adeno-associated virus (AAV php. eb) vector-mediated overexpression of ACAA1 WT and p.N299S in APP^{swe}/PSEN1 Δ E9 (APP/PS1 Δ E9) mice. The APP/PS1 Δ E9 mouse line contains human APP pathogenic mutations (Swedish mutations K595N/M596L) and mutated PSEN1/PS1 (presenilin 1) lacking exon 9.⁴⁷ The AAV overexpression system is safe for gene delivery to the brains of rodents, monkeys, and humans.^{48–50} The AAV php. eb vectors expressing either green fluorescent protein (GFP) (AAV-Vector) or codon-optimized GFP-tagged human ACAA1 WT (AAV-ACAA1 WT) and ACAA1 p.N299S (AAV-ACAA1 N299S) under the control of the cytomegalovirus (CMV) promoter (Supplementary Fig. S6a) were bilaterally injected into the hippocampus region of presymptomatic APP/PS1 Δ E9 mice and WT littermates (3-month-old), respectively. As the spatial memory impairments and

progressive A β plaque deposition in APP/PS1 Δ E9 mice occurred at about at 15–17 weeks⁵¹ and 5–6 months of age,^{47,52} respectively, we assessed the effects of ACAA1 WT and ACAA1 p.N299S overexpression on the behavioral performance in APP/PS1 Δ E9 mice and WT littermates 5 months later after AAV delivery.

In an exploratory open field test, the WT littermates injected with AAV-Vector and AAV-ACAA1 WT showed similar levels of habituation ability in detecting novel environments during the 3-day training course, whereas AAV-ACAA1 N299S-injected WT littermates showed a lower habituation ability compared to those injected with AAV-ACAA1 WT (Fig. 3a). The APP/PS1 Δ E9 mice had an overall lower habituation ability to the testing environment compared to the WT littermates for each treatment. Consistent with the pattern in WT littermates, APP/PS1 Δ E9 mice injected with AAV-Vector and AAV-ACAA1 WT showed the same habituation pattern, but the AAV-ACAA1 N299S-injected APP/PS1 Δ E9 mice exhibited a significantly impaired habituation ability to the novel environment compared to the APP/PS1 Δ E9 mice injected with AAV-Vector or AAV-ACAA1 WT (Fig. 3a).

The memory formation and retrieval abilities of the APP/PS1 Δ E9 mice injected with AAV-ACAA1 WT and AAV-ACAA1 N299S were assessed by using the contextual fear conditioning test, in which their freezing responses were quantified at 1 and 7 days after the administration of an electric shock.⁵³ Compared to the WT littermates, the APP/PS1 Δ E9 mice had a reduction of freezing behavior at both 1 and 7 days after the electric shock, suggesting an impaired contextual retrieval of fear memory (Fig. 3b). The APP/PS1 Δ E9 mice or WT littermates injected with AAV-ACAA1 WT had no significant alterations of freezing performance at both 1 and 7 days after the electric shock compared to the respective group injected with AAV-Vector group (Fig. 3b), although there is a tendency for better effect of AAV-ACAA1 WT in APP/PS1 Δ E9 mice. Delivery of AAV-ACAA1 N299S aggravated the impaired freezing responses in the APP/PS1 Δ E9 mice and WT littermates compared to the respective group injected with AAV-ACAA1 WT at both testing time points (Fig. 3b).

To look further at the subsequent consequences of AAV-ACAA1 WT or AAV-ACAA1 N299S delivery on spatial learning and memory, we carried out a Morris water maze place navigation task with these animals (Fig. 3c, d). Comparable swimming speed was found in all the groups of the APP/PS1 Δ E9 mice and their WT littermates regardless of the injection with AAV-ACAA1 WT or AAV-ACAA1 N299S, which indicated no significant neuromotor differences among the groups (Fig. 3c). Although all APP/PS1 Δ E9 mice and WT littermates managed the task after a 7-day training period, a significantly impaired learning ability was observed in APP/PS1 Δ E9 mice compared to their WT littermates (Fig. 3c), consistent with our previous study⁵⁴ and others.⁵⁵ We observed a significantly impaired learning in the APP/PS1 Δ E9 mice given the AAV-ACAA1 N299S compared to these injected AAV-ACAA1 WT or AAV-Vector (Fig. 3c), and a similar pattern was observed in the WT littermate groups. A 4-h and a 72-h probe trials after the last training session were further performed to evaluate impairment of short- and long-term memory for spatial reference, respectively. A greater memory loss was found in APP/PS1 Δ E9 mice compared to WT littermates injected with AAV-Vector (using percentage of time, percentage of distance in the target quadrant, and the number of platform location crosses as readouts; Fig. 3d). The WT littermates treated with AAV-Vector, AAV-ACAA1 WT, or AAV-ACAA1 N299S exhibited similar preferences for both tests, except for the AAV-ACAA1 N299S group that had fewer platform location crosses compared to the AAV-ACAA1 WT group (Fig. 3d). Intriguingly, AAV-ACAA1 N299S-treated APP/PS1 Δ E9 mice had inferior preference for the target quadrant relative to the APP/PS1 Δ E9 AAV-ACAA1 WT group, suggesting that memory formation deficits in APP/PS1 Δ E9 mice were exacerbated by ACAA1 p.N299S overexpression. The number of platform location crosses was significantly increased in the AAV-ACAA1 WT group compared



to the AAV-Vector group in APP/PS1ΔE9 mice in the 72-h probe trial, indicating potentially beneficial effect of delay in the development of AD in this murine model (Fig. 3d). Taken together, these behavioral tests suggested a detrimental effect of ACAA1 p. N299S during the memory consolidation phase.

Overexpression of ACAA1 p.N299S accelerated AD pathology in APP/PS1ΔE9 mice
We examined the AD pathological changes in the brain tissues of APP/PS1ΔE9 mice with delivery of ACAA1 WT and ACAA1 p.N299S at 6 months after AAV injection. Consistent with the injection

Fig. 3 ACAA1 p.N299S aggravated memory impairments in APP/PS1 Δ E9 mice. **a** Impaired habituation in the exploratory open field for APP/PS1 mice (8-month-old) and wild-type littermates with delivery of AAV-ACAA1 N299S versus AAV-ACAA1 WT or empty vector. The changes of distance traveled on days 2 and 3 were normalized to the distance traveled on day 1 of training. Data are mean \pm SEM. ns, not significant; * P < 0.05; ** P < 0.01, two-way repeated-measures ANOVA. **b** ACAA1 p.N299S accelerated memory retrieval impairment of APP/PS1 and WT mice in fear conditioning tests. Shown data are the percentages of freezing time after 1 day (left) and 7 days (right) of electric shocks. Data are mean \pm SEM. ns, not significant; * P < 0.05; ** P < 0.01, one-way ANOVA with the Tukey's post hoc test. **c, d** Morris water maze tests of APP/PS1 Δ E9 mice or WT littermates with delivery of AAV empty vector or AAV-mediated expression of ACAA1 WT and ACAA1 N299S. The APP/PS1 Δ E9 mice or WT littermates with AAV-Vector, AAV-ACAA1 WT, or AAV-ACAA1 N299S injection showed differences in escape latency, path length, and swim speed during learning session (c) and in probe trial performance at 4 h (short-term memory; left panel) and at 72 h (right panel) (d). TQ target quadrant (percentage of time and percentage of distance in the target quadrant), OQ opposite quadrant. Bars represent mean \pm SEM. * P < 0.05; ** P < 0.01; one-way ANOVA with the Tukey's post hoc test

location, immunohistochemistry using a GFP-tag-specific antibody showed a widespread overexpression of ACAA1 WT and ACAA1 p.N299S in the hippocampus tissues, with prominent expression of ACAA1-GFP in the neurons of the CA1, CA2, and CA3 regions, especially within the CA3 subfield (Fig. 4a). As ACAA1 expression was driven by the CMV promoter, ACAA1-GFP expression had no cell-specific pattern and was detectable in both neuronal cells (positive immunostaining against NeuN [RBFOX3, RNA binding fox-1 homolog 3] and GFP) and microglia (positive immunostaining against IBA1 [AIF1, allograft inflammatory factor 1] and GFP) (Fig. 4a).

Measurement of soluble and insoluble A β levels by using enzyme-linked immunosorbent assay (ELISA) showed that soluble A β 42/A β 1-42 species, which are synaptotoxic in AD,⁵⁶ were significantly increased in both the hippocampus and cortex tissues of APP/PS1 Δ E9 mice with overexpression of ACAA1 p.N299S relative to the ACAA1 WT group (Fig. 4b). The levels of insoluble A β 42 were also increased in the hippocampus, but not in the cortex tissues of APP/PS1 Δ E9 mice injected with AAV-ACAA1 p.N299S relative to AAV-ACAA1 WT (Fig. 4b). However, both soluble and insoluble A β 40/A β 1-40 species were not significantly changed in the hippocampus and cortex tissues of the ACAA1 p.N299S group compared to the ACAA1 WT group. Overexpression of ACAA1 WT could reduce the level of soluble A β 40 compared to the empty vector group in the hippocampus tissues of APP/PS1 Δ E9 mice (Fig. 4b).

We assessed the effect of ACAA1 p.N299S overexpression on amyloid deposition by using A β (antibody 4G8) immunostaining and quantified the area covered by A β plaques in both the hippocampus and cortex tissues of APP/PS1 Δ E9 mice. A significantly increased burden of 4G8-labeled A β plaques was observed in hippocampus and cortex tissues of APP/PS1 Δ E9 mice after delivery of ACAA1 p.N299S compared to those groups injected with the empty vector and ACAA1 WT (Fig. 4c, d). Similar to the ELISA results for soluble A β 40 and insoluble A β 42, delivery of ACAA1 WT reduced the number of A β plaques compared to the empty vector in the hippocampus tissue of APP/PS1 Δ E9 mice. Immunohistochemical staining analysis also showed a significant increase of 4G8-labeled A β plaque burden in coronal brain sections of APP/PS1 Δ E9 mice after AAV-ACAA1 N299S injection compared to those with AAV-ACAA1 WT injection (Supplementary Fig. S6b, c). Together, all these findings demonstrated that overexpression of ACAA1 p.N299S accelerated A β pathology in APP/PS1 Δ E9 mice.

Overexpression of ACAA1 p.N299S caused neuron loss in the hippocampal CA3 region and disturbed synaptic function. We examined hippocampal morphology of neuronal cells using hematoxylin and eosin (H&E) staining and Nissl staining to discern the deleterious effect of ACAA1 p.N299S. The number of neurons in the hippocampal CA3 region was significantly decreased in the WT littermates and APP/PS1 Δ E9 mice with delivery of AAV-ACAA1 N299S compared to the respective group with AAV-ACAA1 WT. H&E staining and Nissl staining of brain sections also showed a significant shrinkage of the hippocampus CA3 region in animals

with AAV-ACAA1 N299S injection (Fig. 5a, b). The number of NeuN (neuron marker)-positive neuronal cells in the hippocampus CA3 region of WT littermates and APP/PS1 Δ E9 mice injected with AAV-ACAA1 N299S was also significantly decreased compared to the respective group with AAV-ACAA1 WT (Fig. 5a, b). These results indicated that ACAA1 p.N299S overexpression induced neuronal loss.

Consistent with the decreased levels of structural neuroplasticity markers PSD-95 and SYP in HM cells and U251-APP cells with overexpression of ACAA1 p.N299S relative to cells overexpressing ACAA1 WT (Fig. 2d, e), the levels of these proteins were significantly decreased in hippocampus tissues of WT littermates and APP/PS1 Δ E9 mice after the delivery of AAV-ACAA1 N299S compared to AAV-ACAA1 WT (Fig. 5c, d). This effect was also consistent with the effect of ACAA1 KO in HM cells and U251-APP cells (Supplementary Fig. S3), indicating ACAA1 p.N299S as a loss-of-function mutation. Moreover, the levels of these proteins that are actively involved in synaptic plasticity, such as NeuN, GluR1, GluR1 (pS831), and GRIN2B, were also decreased in the hippocampus tissues of WT littermates and APP/PS1 Δ E9 mice after AAV-ACAA1 p.N299S delivery compared to the respective group injected with AAV-ACAA1 WT (Fig. 5c, d).

Acceleration of A β pathology by ACAA1 p.N299S was mediated by impaired lysosomal function

Dysfunction of the lysosome and autophagy has been actively involved in neurodegeneration.^{46,57-59} Overexpression of ACAA1 p.N299S or ACAA1 KO in HM cells and U251-APP cells decreased lysosomal marker proteins LAMP1 and LAMP2A and increased LC3-II:LC3-I ratio and SQSTM1 protein level (Supplementary Figs. 2d, e and S3c, d), and this observation could be validated in SH-SY5Y cells (Supplementary Fig. S5), suggesting reduced lysosomal activity caused by ACAA1 p.N299S or ACAA1 KO. We next tested whether the increased level of A β in APP/PS1 Δ E9 mice with delivery of ACAA1 p.N299S (Figs. 4 and Supplementary Fig. S6b, c) was associated with lysosomal dysfunction. We quantified the LAMP1 and LAMP2A protein levels in hippocampus tissues of APP/PS1 Δ E9 mice and WT littermates injected with AAV-ACAA1 WT and AAV-ACAA1 N299S. Overexpression of ACAA1 p.N299S caused a significant decrease of LAMP1 and LAMP2A in the hippocampus tissues compared to overexpression of ACAA1 WT in APP/PS1 Δ E9 mice and WT littermates, respectively (Fig. 6a, b). Similarly, overexpression of ACAA1 p.N299S led to an increased LC3-II:LC3-I ratio and SQSTM1 protein level in the hippocampus tissues of APP/PS1 Δ E9 mice and WT littermates compared to the respective group with ACAA1 WT overexpression (Fig. 6a, b).

To test whether the increased A β accumulation upon ACAA1 p.N299S overexpression was caused by lysosomal dysfunction and autolysosome defect, we used BAF1 and NH4CL, inhibitors of the vacuolar (V)-type ATPase that results in blockage of autophagosome-lysosome fusion and accumulation of LC3B,^{60,61} as the positive controls to treat U251-APP cells and determined the level of A β in cell culture supernatant. Lysosomal function was inhibited in U251-APP cells (Fig. 6c) and HM cells (Supplementary Fig. S7a) by BAF1 and NH4CL treatments, as well as in cells

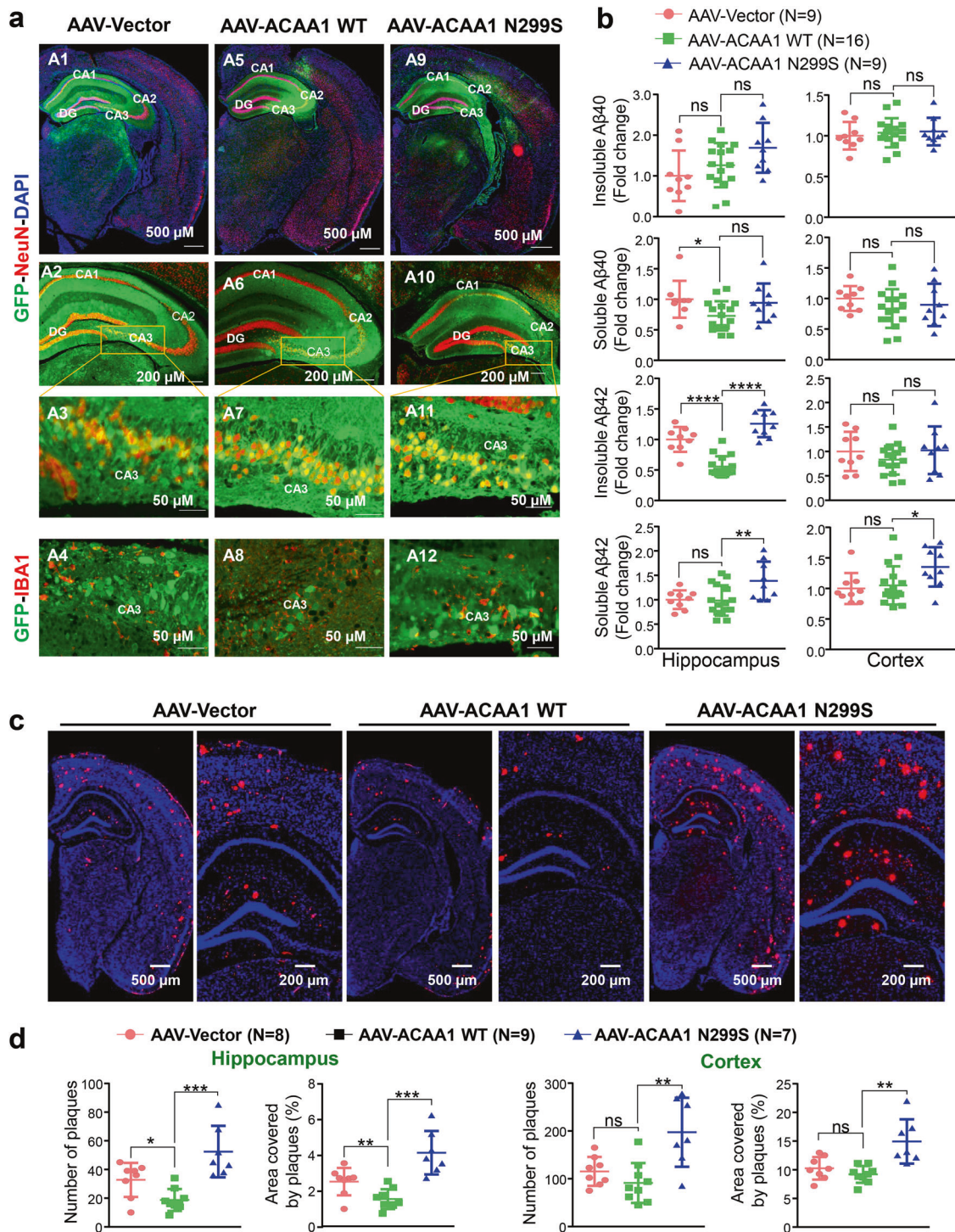


Fig. 4 Overexpression of ACAA1 p.N299S via adeno-associated virus delivery exacerbated amyloid- β ($A\beta$) pathology. APP/PS1 Δ E9 mice and WT littermates were injected with AAV-Vector, AAV-ACAA1 WT, or AAV-ACAA1 N299S at 3 months of age and sacrificed at 9 months of age. **a** Fluorescent signals in the brain section of a 9-month-old mouse receiving AAV-Vector, AAV-ACAA1 WT, or AAV-ACAA1 N299S. **b** Quantification of soluble and insoluble $A\beta$ 40 and $A\beta$ 42 in the hippocampus and cortex tissues of mice in **a** by ELISA. **c**, **d** Representative microphotographs of hippocampal sections stained with an 4G8-specific $A\beta$ antibody (**c**), and quantitative analysis of the number of $A\beta$ plaques shown by 4G8 immunoreactivity in hippocampal and cortex tissues in APP/PS1 Δ E9 mice (**d**). Bars represent mean \pm SD. ns, not significant; * P < 0.05; ** P < 0.01; *** P < 0.001; **** P < 0.0001; Student's t test

overexpressing ACAA1 p.N299S or ACAA1 KO, as indicated by the decreased lysosomal protease activities according to the β - N -acetylglucosaminidase (NAG) assays. This dysfunction effect was accompanied by increased extracellular $A\beta$ 40 and $A\beta$ 42 levels in

comparison with untreated cells (Fig. 6d). Treatment of BAF1A1 (200 nM) and NH₄CL (10 mM) alone raised the extracellular $A\beta$ 40 and $A\beta$ 42 levels compared to untreated cells (Fig. 6d), and this effect was comparable to the cells overexpressing ACAA1

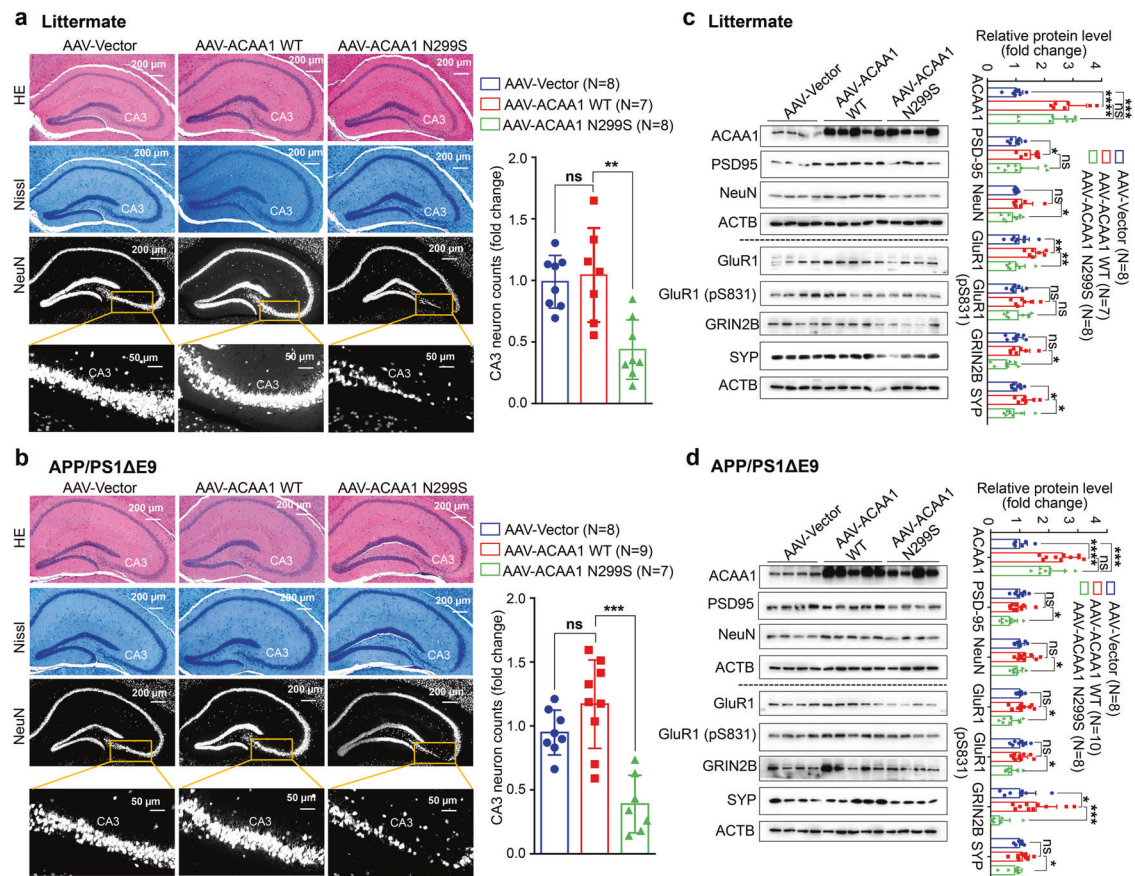


Fig. 5 Overexpression of ACAA1 p.N299S in APP/PS1ΔE9 mice and WT littermates induced neuronal losses. **a, b** Neuronal loss in the CA3 region of hippocampus in WT littermates (**a**) and APP/PS1ΔE9 mice (**b**) after delivery of the AAV-Vector, AAV-ACAA1 WT, and AAV-ACAA1 N299S. Higher neuronal density, marked by NeuN antibody, was noted in mice overexpressing ACAA1 p.N299S, suggesting a potential decrease of neurogenesis or an increase of neuron loss. Immunostaining of brain sections was performed using NeuN antibody. Shown results are representative hematoxylin and eosin (H&E) staining (top), Nissl staining (middle), and NeuN staining (bottom) of mouse hippocampus tissues in each group. **c, d** Decreased protein levels of structural plasticity markers SYP, PSD95, NeuN, GluR1, GluR1 (pS831), and GRIN2B in the hippocampus tissues of WT littermates (**c**) and APP/PS1ΔE9 (**d**) mice with AAV-mediated expression of ACAA1 and its mutant. Bars represent mean ± SD. ns, not significant; * $P < 0.05$; ** $P < 0.01$; *** $P < 0.001$; **** $P < 0.0001$; Student's *t* test

p.N299S or with ACAA1 KO. Concordantly, overexpression of ACAA1 p.N299S inhibited lysosomal function and autophagosome–lysosome fusion in U251-APP cells (Supplementary Fig. S7b) and HM cells (Supplementary Fig. S7c), and this effect was similar to that of ACAA1 KO or BAF1 and NH4CL treatments (Supplementary Fig. S7b, c).

We performed rescue experiments using the U251-APP and HM ACAA1 KO cells. Overexpression of ACAA1 WT rescued the altered LC3-II:LC3-I ratio and SQSTM1 protein level (Figs. 6e and Supplementary Fig. S7d) and lysosomal activity (Figs. 6f and Supplementary Fig. S7e) in ACAA1 KO cells, whereas ACAA1 p.N299S overexpression had no such an effect. Accordingly, overexpression of ACAA1 WT, but not ACAA1 p.N299S, ablated the increased extracellular Aβ40 and Aβ42 levels in U251-APP ACAA1 KO cells (Fig. 6g). As the Aβ42:Aβ40 ratio was not significantly changed in these conditions, we measured the protein levels of BACE1, PSEN1, PSEN2, and PEN2 in U251-APP cells with or without the respective treatment and transfection. We found no significant alterations of BACE1, PSEN1, PSEN2, and PEN2 protein levels between cells with or without ACAA1 KO. Similarly, no difference of these protein levels was found between cells with or without chemical treatments or between cells with overexpression of ACAA1 WT and p.N299S (Supplementary Fig. S7f). This result suggested that the increased levels of Aβ40 and Aβ42

in cells with ACAA1 KO or ACAA1 p.N299S overexpression might be caused by the lysosomal dysfunction and impaired autophagosome–lysosome fusion. Together, these findings demonstrated that ACAA1 p.N299S accelerates Aβ burden.

Overexpression of ACAA1 p.N299S affected excitatory synaptic transmission

As ACAA1 p.N299S overexpression reduced the structural neural protein levels and was associated with Aβ accumulation, we determined whether this mutation directly alters excitatory neuron synaptic transmission. We used rat hippocampal CA1 pyramidal neurons and dual whole-cell recordings described in our previous studies,^{21,62} to investigate the electrophysiological effect of ACAA1 WT and p.N299S. Compared to the control neurons, overexpression of ACAA1 WT decreased the AMPA receptor (AMPA)-mediated synaptic transmission (Fig. 7a), whereas ACAA1 p.N299S had no such an effect (Fig. 7b). Similarly, the *N*-methyl-D-aspartate receptor (NMDAR)-mediated synaptic transmission was inhibited significantly by overexpression of ACAA1 WT, but overexpression of ACAA1 p.N299S did not change NMDAR-evoked excitatory postsynaptic currents (EPSCs) (Fig. 7c, d). Overexpression of ACAA1 WT, but not ACAA1 p.N299S, decreased the ratio of AMPAR and NMDAR-mediated EPSCs when compared to neighboring wild-type neurons in respective assays

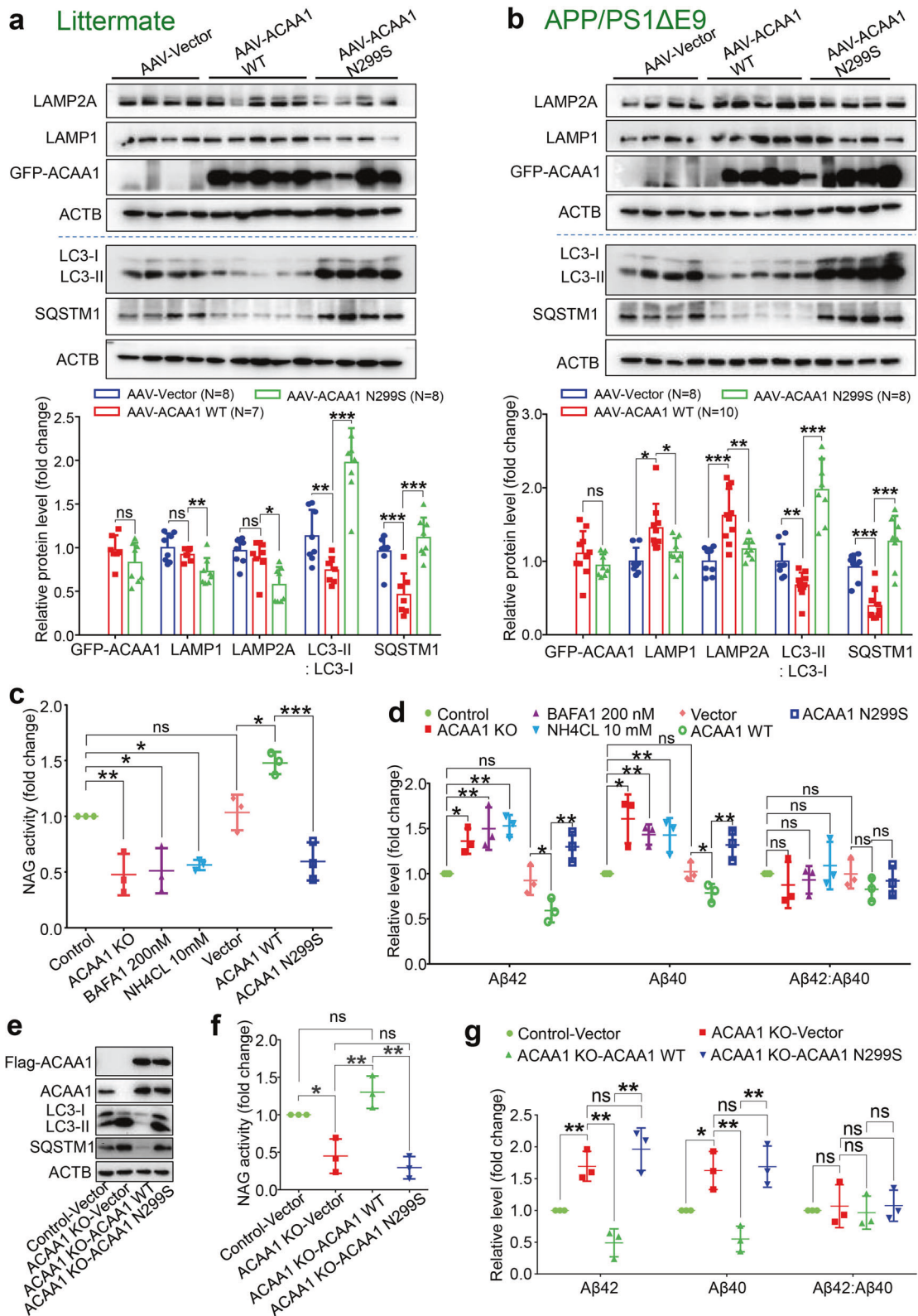


(Fig. 7e, f). Nonetheless, both ACAA1 WT and p.N299S over-expression did not affect the paired-pulse ratio (Fig. 7g, h), which reflects presynaptic release probability. Collectively, these results suggested that ACAA1 WT had an active role in modulating the excitatory synaptic transmission mediated by both AMPAR and

NMDAR in neurons, whereas ACAA1 p.N299S impaired this regulation possibly via altered levels of proteins involved in synaptic functions (Fig. 5) and/or a gain of toxic function. Focused experiments should be performed to test this hypothesis and to elucidate the underlying mechanism.

Fig. 6 Effect of ACAA1 p.N299S on A β pathology was mediated by lysosomal dysfunction. **a, b** Western blot analysis of lysosomal proteins LAMP1 and LAMP2A and autophagy markers LC3-II:LC3-I ratio and SQSTM1 in the hippocampus tissues of WT littermates (**a**) and APP/PS1 Δ E9 (**b**) injected with AAV-ACAAA WT or AAV-ACAAA N299S. Bars represent mean \pm SD. ns, not significant; * P < 0.05; ** P < 0.01; *** P < 0.001; Student's *t* test. **(c)** ACAA1 knockout (KO) or overexpression of ACAA1 p.N299S in U251-APP cells decreased NAG activity. Cells were treated with BAF1A1 (200 nM), NH4CL (10 mM), or without treatment (Control) or were transfected with empty vector (Vector) and expression vector of ACAA1 WT, or ACAA1 p.N299S. **d** Levels of extracellular A β 42, A β 40, and A β 42:A β 40 ratio in the culture supernatants of U251-APP cells and U251-APP ACAA1 KO cells. **e–g** Overexpression of ACAA1 WT, but not ACAA1 p.N299S, in U251-APP ACAA1 KO cells had a rescuing effect on the altered protein levels of autophagy markers (**e**), lysosomal markers (**f**), and the levels of extracellular A β 42 and A β 40 in the culture supernatant (**g**). The U251-APP cells without ACAA1 knockout was used as a control, and cells were transfected with empty vector (Vector) and expression vector of ACAA1 WT or ACAA1 p.N299S. Data in **e–g** were based on three independent experiments. Bars represent mean \pm SD. ns, not significant; * P < 0.05; ** P < 0.01; *** P < 0.001; Student's *t* test

DISCUSSION

Accumulating evidence has shown that AD has a genetic basis, with contributions from multiple causal and risk genes.^{13,14,17,22} Molecular characterization of these genes provides insights into understanding AD pathobiology and developing drug therapy. In this study, we identified an association of the missense variant ACAA1 p.N299S with AD in EOFAD patients (Fig. 1a and Supplementary Table S2), which showed a population-specific pattern. We have further provided *in vitro* and *in vivo* data showing that this ACAA1 variant facilitates A β pathology and exacerbates cognitive decline by impairing lysosomal and synaptic function, adding this gene to the current list of AD risk and causal genes.^{13,14,17,22,41} ACAA1 p.N299S is a loss-of-function mutant, as it decreases enzymatic activity (Fig. 1b) and causes a catastrophic cascade with the involvement of disturbed global gene expression pattern and impaired lysosomal, autolysosomal, and synaptic functions (Fig. 2). Using AAV-mediated overexpression of ACAA1 p.N299S in APP/PS1 Δ E9 mice exacerbated cognition decline (Fig. 3), accelerated A β pathology (Figs. 4, 6 and S6), and impaired synaptic protein expression and neuronal loss in the hippocampus CA3 region (Fig. 5). Moreover, overexpression of ACAA1 p.N299S disturbed the excitatory synaptic transmission in rat hippocampus Purkinje neurons as compared to ACAA1 WT (Fig. 7). All these results were compatible with the impaired lysosomal function and autophagosome–lysosome fusion that were caused by the ACAA1 p.N299S (Fig. 8).

The involvement of ACAA1 in lipid metabolism as part of the development of AD can be explained and has many important implications. First, previous studies had shown that lipids are crucial for maintaining neuronal development, synaptic plasticity, and function.^{63,64} Abnormal lipid metabolism is actively involved in the development of neurodegenerative diseases, including AD.^{65,66} Moreover, dysfunction of VLCFA β -oxidation in peroxisomes is a common feature of some neurodegenerative diseases,^{67,68} although the molecular underpinning underlying the neuron loss vary widely.^{68,69} In particular, peroxisomal function declines with age and is linked to AD,^{69,70} with an increased levels of VLCFAs in the AD brains,⁶⁹ suggesting a possible defect in peroxisomal β -oxidation during the development of AD. Second, numerous studies have demonstrated that loss of peroxisomal proteins and enzymes constitutes one of the reasons for severe neuronal defects,^{71,72} as peroxisomes are common in these neuronal cells, such as neurons, astrocytes, oligodendrocytes, microglia, and Schwann cells.^{73,74} Indeed, mice lacking the peroxisomal proteins PEX5⁷⁵ and PEX10⁷⁶ display severe neurological defects. Loss-of-function mutations in ACOX1 (acyl-CoA oxidase 1), the first and rate-limiting enzyme of the VLCFA β -oxidation signaling pathway in peroxisomes, impair synaptic transmission and cause glial and axonal loss.⁷⁷ Similarly, mice deficient for MFP2, a VLCFA metabolizing enzyme upstream of ACAA1, also exhibit a severe loss of axons.⁷⁸ Impairment of axons has been frequently found in AD.^{79,80} Third, peroxisomal ACAA1 is the last and key enzyme in VLCFA β -oxidation and a main acetyl-CoA producer.^{81,82} The reduction of peroxisomal ACAA1 enzymatic activity decreases the rate of peroxisomal β -oxidation of

palmitoyl-CoA.⁸³ It has been reported that ACAA1 deficiency leads to pseudo-Zellweger syndrome,^{83,84} and emerging evidence has shown that AD and pseudo-Zellweger syndrome share a common risk of peroxisomal alterations.^{69,85} Therefore, our finding of ACAA1 p.N299S, a loss-of-function mutation in EOFAD patients, to be actively involved in A β pathology and cognitive decline in an AD murine model, further emphasizes the important role of peroxisomal protein dysfunction in neurodegeneration.

Dysfunctions in the lysosomal system are well-recognized early neuropathological features of AD, marked by prominent enlargement of endosomal compartments and lysosomal deficits.^{59,86,87} Lysosomes are major cellular degradative organelles, involved in turnover of molecular cargo from both autophagic and endocytic pathways,⁸⁷ and in AD, disturbed lysosomal degradation is presumed to be of key importance in aberrant autophagic vacuole turnover.^{86,88} The lysosomal deficits in AD are thought to cause impaired autophagosome–lysosome fusion and disruption of substrate proteolysis within autolysosomes.^{57–59,86} Defective lysosomal proteolysis exacerbates A β pathology in mouse models of AD.^{57,59,86} We found that ACAA1 p.N299S impaired lysosomal function and cognitive function in both WT littermates and APP/PS1 Δ E9 mice, suggesting that defective lysosomal production in neuropathology might be a common feature in neurodegenerative disease. The elimination of A β generated in the endocytic–autophagic pathways in neurons has a dependence on lysosomal degradation capacity.^{57,89} Consistent with this speculation, we found that ACAA1 p.N299S causes lysosomal inhibition, lead to an increased A β load, impaired synaptic function, and accelerated neuronal loss in AD. Importantly, AAV-ACAAA1 p.N299S treatment leads to an impairment of spatial reference memory. The significant increment of soluble and insoluble A β 42 and plaque burden, resulting in excessive A β neurotoxicity⁵⁴ and lysosomal dysfunction in APP/PS1 Δ E9 mice upon ACAA1 p.N299S overexpression, may account for the accelerated neuronal loss in APP/PS1 Δ E9 mice with the administration of AAV-ACAAA1 p.N299S. It should be mentioned that ACAA1 p.N299S also caused neuronal loss in WT littermates (Fig. 5a), which suggested that other factors caused by ACAA1 p.N299S were involved in this process. Further study should be carried out to confirm this speculation. We provided multiple lines of evidence to show that overexpression of ACAA1 p.N299S in APP/PS1 Δ E9 mice significantly aggravated A β pathologies and A β -mediated neurodegeneration, supporting ACAA1 as a sensitizing factor for A β pathology and as a novel mechanism underlying the AD risk.

Neurotoxic A β oligomers can interact with and activate NMDA receptor^{90,91} and affect NMDA receptor signaling.^{90,92,93} Over-activation of NMDA receptors causes excitotoxicity and neuronal cell damage,⁹⁴ whereas chronic NMDA receptor hyperactivity contributes to neuron loss in the development of AD.⁹⁵ The Food and Drug Administration-approved drugs for treating AD, such as rivastigmine, galantamine, donepezil, memantine, memantine-donepezil combination, and tacrine, block glutamate NMDAR, inhibit acetylcholinesterase, or have a combination of both effects. We found that ACAA1 WT likely inhibited the excitatory synaptic

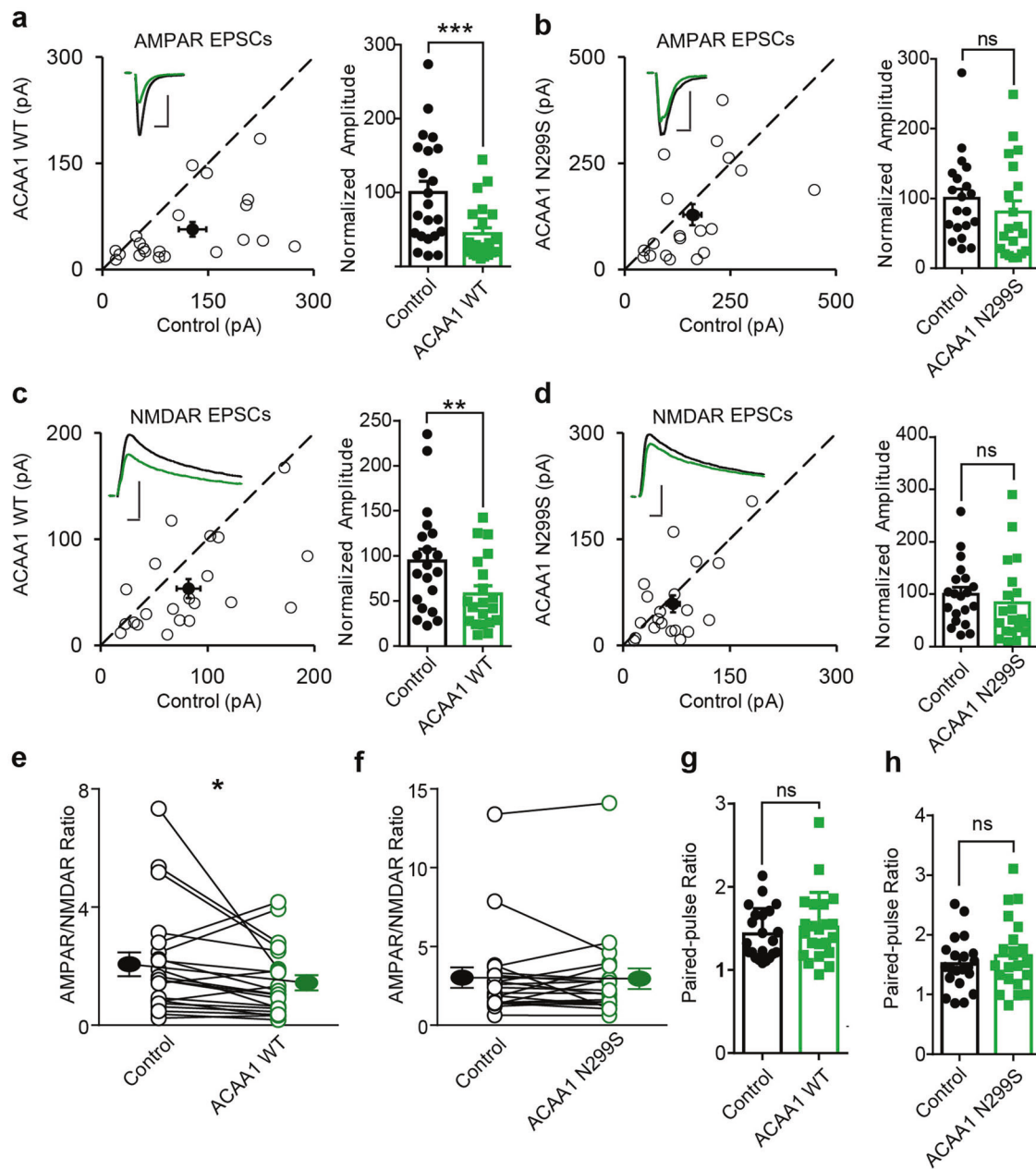


Fig. 7 ACAA1 p.N299S disturbs its physiological regulation of excitatory synaptic transmission. **a–d** Rat hippocampal slice cultures were biolistically transfected with expression vector of ACAA1 WT or ACAA1 p.N299S. Simultaneous dual whole-cell recordings were performed in a transfected CA1 pyramidal neuron (green trace) and a neighboring wild-type one (black trace). The evoked AMPA (**a, b**) and NMDA (**c, d**) EPSCs were measured, and open and filled circles represent amplitudes for single pairs and mean \pm SEM, respectively. Sample current traces from control (black) and experimental (green) cells are shown as insets. Bar graphs show normalized EPSC amplitudes (mean \pm SEM) of -70 mV (**a**, $***P < 0.001$; **b**, $P > 0.05$) and $+40$ mV (**c**, $**P < 0.005$; **d**, $P > 0.05$) presented in scatter plots. The scale bars for representative EPSC traces are 100 pA/25 ms (**a**) and 50 pA/25 ms (**b–d**). **e, f** Difference of AMPA/NMDA ratios recorded from neurons overexpressing ACAA1 WT ($*P < 0.05$) or ACAA1 p.N299S ($P > 0.05$) compared to the respective wild-type (Control) ones. **g, h** No change in paired-pulse ratio of the second EPSC over the first EPSC from neurons overexpressing ACAA1 WT ($P > 0.05$) or ACAA1 p.N299S ($P > 0.05$) relative to the control neurons. All the statistical differences are estimated relative to the respective control neurons, with a two-tailed Wilcoxon signed-rank sum test

transmission, whereas ACAA1 p.N299S impaired this regulation (Fig. 7). We speculated that ACAA1 p.N299S contributes to AD by disrupting the essential regulation of ACAA1 WT on the excitatory synaptic transmission via a currently unknown mechanism that awaits future focused assays. It would be rewarding to find whether ACAA1 can be a potential target in AD therapeutics, as overexpression of ACAA1 WT seems to have a beneficial role in reducing A β load and for maintaining presynaptic and post-synaptic integrity and function (Figs. 4 and 5).

This study had several limitations. First, the association of ACAA1 p.N299S with EOFAD had to be validated in independent populations and detailed analyses of clinical features of those AD patients carrying this mutation should be performed. Second, we found that p.N299S impairs the enzymatic activity of ACAA1, but the detailed mechanism as to how the reduced ACAA1 enzymatic activity is involved in the progress of AD and whether the lysosomal dysfunction induced by ACAA1 p.N299S has any cell-type specificities in the brain have not been sufficiently elucidated.

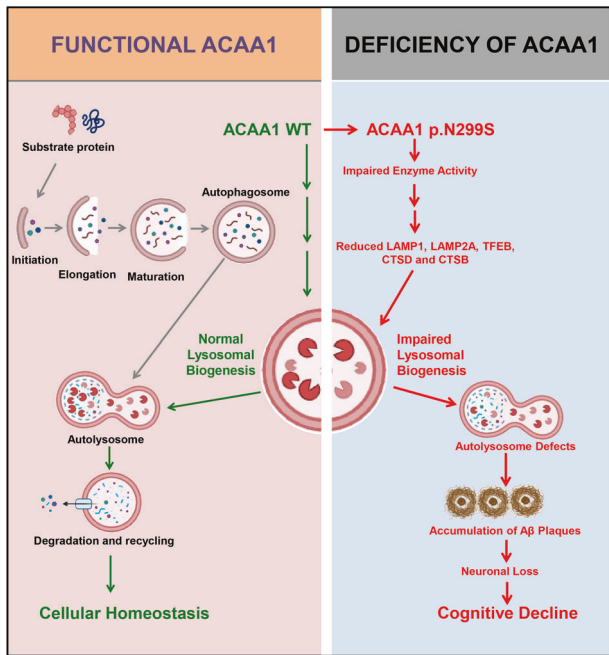


Fig. 8 A proposed role of the ACAA1 p.N299S-mediated lysosomal dysfunction and impaired autophagy in the development of AD. ACAA1 p.N299S has an impaired enzymatic activity, affects autophagy and lysosomal function, subsequently contributes to the aggravation of the A β pathology and neuronal loss, and finally causes cognitive impairment and other AD-related symptoms

Although the transcriptomic gene profiling in this study could offer some hints regarding the alterations of pathways and AD-centered network, the underlying pathway for lysosomal dysfunction caused by reduced peroxisomal ACAA1 activity has remained to be characterized. The altered protein levels of LC3-II/LC3-I and SQSTM1 in cells with or without BAF1 and NH4CL treatment might be compatible with impaired autophagosome–lysosome fusion that was associated with abnormal A β 42 deposition (Figs. 6 and Supplementary Fig. S7). However, we did not perform a focused assay for autophagic flux in cells overexpressing ACAA1 p.N299S or with ACAA1 KO to characterize the potential role of autophagy due to technical reasons, especially considering the fact that we observed an increased LC3-II:LC3-I ratio and SQSTM1 protein level in both ACAA1-deficient cells or cells overexpressing the mutant. Third, although the AAV-mediated gene delivery might have some disadvantages as compared to knock-in animals for characterizing the consequence of ACAA1 p.N299S, we observed remarkable deficits in APP/PS1 Δ E9 mice with AAV-ACAA1 p.N299S as compared to those with AAV-ACAA1 WT, such as cognition decline, A β accumulation, and neuronal loss (Figs. 3–6 and Supplementary Fig. S6), which indicated the deleterious effect of ACAA1 p.N299S. Given the fact that neurons play key roles in AD and interactions between neurons and glial cells are actively involved in the pathobiology of AD,^{65,96} it would be worthwhile to detect the lysosomal and synaptic dysfunctions caused by ACAA1 p.N299S in neuronal cells and neuron–glia interaction models. Fourth, we did not analyze the role of tau in producing these effects mediated by ACAA1 p.N299S, which should be evaluated in future studies by incorporating tau into these models to determine whether ACAA1 p.N299S influences A β and tau during the progression of AD. Finally, we did not perform a drug screening using the ACAA1 as the target. Based on the current results that the WT littermates with AAV-ACAA1 N299S delivery already showed some deficits (Fig. 3), potential chemicals/drugs promoting lysosomal function and/or regulating the excitatory synaptic transmission (Fig. 7) could be expected to

have an ameliorating effect on alleviating the deficits caused by ACAA1 p.N299S and other potentially pathogenic mutations in this gene. The complete picture of ACAA1 and its role in AD will be critical for answering the question as to whether this gene can be used as a druggable target for AD treatment.

In conclusion, we have provided multiple lines of supporting evidence showing peroxisomal ACAA1 contributing to abnormal lysosomal function in AD and for studying the causes of lysosomal dysfunction in AD patients. Overexpression of ACAA1 p.N299S has been shown to contribute to AD by disturbing its enzymatic activity, inhibiting the lysosome system, and aggravating the A β pathology and neuronal loss, which finally caused a cognitive impairment in a murine model of AD (Fig. 8). Our findings reveal a fundamental role of peroxisome-mediated lysosomal dysfunction in AD pathogenesis. It will be rewarding to perform a prospective drug study with ACAA1 as a valid druggable target for improving the pathological characteristics and cognitive impairment symptoms in AD patients with deficiency of ACAA1 enzyme activity and impaired VLCFA β -oxidation.

MATERIALS AND METHODS

Antibodies, chemicals, and vectors

Details of primary antibodies, secondary antibodies and chemicals used in this study are listed in Supplementary Table S4. Vectors p3*Flag-CMV-14 (empty vector), p3*Flag-CMV-14-ACAA1 WT (PPL01228-2a) (ACAA1 WT), and p3*Flag-CMV-14-ACAA1 WT (PPL01228-2B) (ACAA1 N299S) were purchased from Public Protein/Plasmid library (Nanjing, Jiangsu).

Human subjects

The members of the EOFAD family from Guizhou, Southwest China were enrolled in this study. The proband II:3 was diagnosed as having AD (age at onset [AAO] <57 years), and his mother I:2 was diagnosed as possibly having AD (AAO <60 years). Both patients had died before we could have a more focused clinical examination (Fig. 1a). The patients were initially diagnosed as having AD by at least two clinical psychiatrists according to the revised National Institute of Neurological and Communicative Disorders and Stroke and the Alzheimer’s Disease and Related Disorders Association criteria^{97–99} and the Diagnostic and Statistical Manual of Mental Disorders (Fourth Edition) as described in our previous studies.^{36,37,100} Samples were collected according to the Declaration of Helsinki, and the informed consents were obtained from the participants or supervisors of the patients. This study was approved by the Institutional Review Board of Kunming Institute of Zoology (KIZ), Chinese Academy of Sciences (CAS; approval numbers SMKX-20170103-01 and SMKX-SQ-20200414-074-02).

WGS of the AD pedigree

Four individuals including the proband from the AD pedigree were subjected to WGS (Fig. 1a) and were processed using the same pipeline described in our previous study.¹⁰¹ Briefly, genomic DNAs were isolated from the peripheral blood by using AxyPrep Blood Genomic DNA Miniprep Kit (Axygen, USA). Deep WGS (~30 \times) was performed at the Novogene Corporation (Tianjin Novogene Technology Co., Ltd.) using Illumina HiSeq 4000 Platform (150 bp paired-ends reads). We removed low-quality bases of raw reads using Trimmomatic-0.32¹⁰² with the parameters “LEADING:3 TRAILING:3 SLIDINGWINDOW:4:15 MINLEN:36.” Quality-filtered reads were mapped to hg19 reference genome (https://www.ncbi.nlm.nih.gov/assembly/GCF_000001405.13/) by BWA version 0.79a.¹⁰³ The aligned BAM files of each sample were sorted by genomic position using SortSam and merged into a single file using MergeSamFiles in picard-tools-1.107 (<https://github.com/broadinstitute/picard>). We used MarkDuplicates in picard-tools-1.107 to mark the duplicate reads for exclusion in

the subsequent analyses. We used GATK version 2.8¹⁰⁴ for calling single-nucleotide variants (SNVs) with the parameters as recommended (http://www.broadinstitute.org/gsa/wiki/index.php/Best_Practice_Variant_Detection_with_the_GATK_v3) and used the GATK UnifiedGenotyper (UG) to estimate genotype likelihoods in this family. To maximize sensitivity and correctness of SNV calling, we set the GATK UG with a Phred quality score > Q10 as a starting point, followed by filter using the GATK Variant Quality Score Recalibration (VQSR) to exclude spurious SNVs caused by sequencing and mapping artifacts. We annotated all variants according to RefSeq gene transcripts (accessed from the UCSC Genome Browser, <http://genome.ucsc.edu>) using our in-house script as previously described.¹⁰¹

We followed the same strategy in our previous studies^{21,30} to identify all rare (MAF ≤ 0.01 in the datasets of the 1000 Genomes Project^{29,32}) and inherited loss-of-function (stop-gain or frame-shift) and damaging missense variants (Supplementary Tables S1 and S2) and used the dbNSFP database¹⁰⁵ for functional prediction and annotation of SNVs. We also used the CADD score,³¹ a method integrating multiple annotations, to evaluate function potential of SNVs.

Cell culture and western blotting

The U251 glioma, HM, and SH-SY5Y cells were introduced from Kunming Cell Bank, KIZ, CAS. The U251-APP cells with stably expression of mutant APP K670N/M671L produced A β under doxorubicin treatment were taken from our previous studies.^{36,37} Western blotting for target proteins were performed using the common approach as described in our previous studies^{54,106} and the respective antibodies listed in Supplementary Table S4. The detailed information regarding cell culture, transfection, and western blotting can be found in the online Supplementary Materials and Methods.

RNA-seq analysis and ACAA1 co-expression network construction We followed a similar pipeline and procedure in our previous studies^{21,41} to conduct the RNA-seq analysis and reconstruct the ACAA1 co-expression network. More details can be found in the online Supplementary Materials and Methods. We took the compiled expression matrix of 269 postmortem brain samples of AD patients from the AlzData database (www.alzdata.org),⁴¹ which contains reported microarray data of four AD brain tissues, including entorhinal cortex, hippocampus, temporal cortex, and frontal cortex,⁴¹ to discern the co-expression pattern of ACAA1. Spearman's correlation coefficients and the Benjamini-Hochberg-adjusted *P* values (P_{adjust}) were calculated using R package *psych*. The ACAA1-centered co-expression network was constructed using genes that are significantly correlated ($P_{\text{adjust}} < 0.0001$) with ACAA1. Fisher's exact test was used to test the enrichment between DEG signatures of cells overexpressing ACAA1 p.N299S and ACAA1 WT or empty vector.

Generation of ACAA1 KO cell

We used the procedure described in our previous studies^{107,108} to KO ACAA1 in the HM and U251-APP cells. Briefly, small guide RNAs (sgRNAs) (ACAA1-sgRNA-F: 5'-CACCGTCCGAGAGAAGCTCGTG G-3'/ACAA1-sgRNA-R: 5'-AAACCCGACGAGCTTCTCGGCAC-3') targeting ACAA1 were annealed and cloned into the pX330-T7 vector expressing mCherry. The HM and U251-APP cells were transfected with this vector carrying the sgRNAs by using Lipofectamine 3000 (Invitrogen, L3000008) for 48 h, then single cells expressing mCherry were sorted and cultured for 3 weeks for expansion. Genomic DNA was isolated from single HM and U251-APP cells with potential ACAA1 KO using AxyPrep Multi-source Genomic DNA Miniprep Kit (Axygen, 26817KC1) and was amplified by using primer pair ACAA1-sgRNA-Fc: 5'-TGTGGTGCCTTTGTCTCCCT-3'/ACAA1-sgRNA-Rc: 5'-CTCCCATCTG ACGAGAAATACCC-3'). Purified PCR products were sequenced by

using primer ACAA1-sgRNA-Fc for mutation(s) introduced by the sgRNAs. We obtained two cell clones with an insertion of adenine (c.184-185insA) that disrupted the translation of the ACAA1 protein and the KO of endogenous ACAA1 protein could be validated by western blot.

Assays for ACAA1 enzymatic activity and lysosomal activity

The enzymatic activities of ACAA1 WT and ACAA1 p.N299S were measured using the Fluorometric Acetyltransferase Activity Assay Kit (Abcam, ab204536), as previously described.³⁵ Briefly, the assay was performed with 5 μ g of pure protein and 100 nM acetoacetyl coenzyme A sodium salt hydrate (Sigma, A1625), and fluorescence was detected at Ex/Em of 380/520 nm. Both ACAA1 WT and ACAA1 p.N299S proteins were extracted using TnT[®] Quick Coupled Transcription/Translation Systems (Promega, L1170) and purified using the His-tag Protein Purification Kit (Beyotime, P2226). Each sample was analyzed in triplicate.

Lysosomal activities were determined by using the NAG assay. Briefly, lysates of HM, HM ACAA1 KO, U251-APP, or U251-APP ACAA1 KO cells treated with or without the indicated chemicals or transfected with the indicated expression vectors were isolated. The NAG assay was performed by using a commercial kit from MIBio (Cat. #SU-B16484) following the manufacturer's instructions.

Mouse models, AAV-mediated gene delivery, behavioral tests, and tissue analyses

The APP/PS1 Δ E9 mice were originally introduced from Jackson Laboratory.⁴⁷ The APP/PS1 Δ E9 mice and WT littermates were bred and maintained at the experimental animal core facility of KIZ on a 12-h light/dark cycle, with free access to food and water. In all experiments, genotypes of both *APP* and *PSEN1* were confirmed by using tail DNA following the standard PCR condition.⁵⁴ Animals were divided into sex- and age-matched groups, and both genders were used for analyses.

We used 3-month-old APP/PS1 Δ E9 mice and WT littermates for AAV-mediated gene delivery. Briefly, the recombinant AAV php.eb vectors with GFP expression (AAV pAV-C-GFP) carrying empty vector (AAV-Vector), ACAA1 WT (AAV-ACAA1 WT) or p.N299S (AAV-ACAA1 N299S) (Supplementary Fig. S6a) were developed by the VIGENE BIOSCIENCES.INC. The original titers of AAV-Vector, AAV-ACAA1 WT, and AAV-ACAA1 N299S were 8.52×10^{13} , 6.68×10^{13} , and 1.01×10^{14} vector genomes (vg)/mL, respectively. The viruses were stored at -80°C and diluted with saline (0.9% sodium chloride) to 5.00×10^{13} vg/mL for injection. Mice were anesthetized by intraperitoneal injection of pentobarbital (0.06 g/kg body weight) and positioned on a stereotactic frame (Panlab HARVARD, MA, USA), then each animal was bilaterally injected with 1 μ L viral solution (5.00×10^{13} vg/mL) into the hippocampus (stereotaxic coordinates: anteroposterior, -2 mm; mediolateral, ± 2.1 mm; dorsoventral, -1.9 mm) with a syringe pump (Panlab, Harvard, MA, USA) at a speed of 200 nL/min. We left the needle in place for an additional 5 min before it was slowly removed. We assessed the effects of AAV-Vector, AAV-ACAA1 WT, and AAV-ACAA1 N299S on behavioral performance in these animals after AAV delivery for 5 months.

The behavioral tests of mice were performed following the previously described protocols.⁵³⁻⁵⁵ For all behavioral tests, the experimenter was blinded to the genotypes of mice. The detailed information of each test can be found in the online Supplementary Materials and Methods.

After behavioral tests, animals (at an age of 9 months) were euthanized for collecting brain tissues. Briefly, the brain was gently removed and rinsed in cold phosphate-buffered saline (PBS; pH 7.4), followed by immediate dissection into two halves. One half was stored at -80°C for biochemistry assays, whereas the other half was fixed in 4% paraformaldehyde in PBS at 4°C for immunohistochemistry and immunofluorescence assays following the previously reported protocol.^{54,106} We followed the previously

reported protocols to isolate plaque-related insoluble and soluble A β in brain tissues for quantification by ELISA.^{54,109} The detailed information for brain dissection, immunohistochemistry, immunofluorescence, and ELISA for A β can be found in the online Supplementary Materials and Methods.

The animal care and experimental protocols were approved by the Institutional Animal Care and Use Committee of KIZ, CAS.

H&E staining and Nissl staining

The brain tissues were paraffin embedded for cutting into 4- μ m sections. Each section was deparaffinized by passing through 100% xylene, then rehydrated through incubation with serial dilutions (100, 95, and 75%) of ethanol (each 10 min). H&E staining and Nissl staining were performed according to the instructions provided by Beyotime Institute of Biotechnology (C0105) and Servicebio (G1032), respectively.

Electrophysiology in slice cultures

The electrophysiology in brain slice cultures was performed following our previously described protocol.^{21,62} The detailed information can be found in the online Supplementary Materials and Methods.

Statistical analysis

The number of samples or animals is specified in the caption for each experiment. Specific statistical analyses were performed according to the requirements of different experimental procedures. For comparison of multiple groups, one-way analysis of variance (ANOVA) followed by Tukey's post hoc tests were used. For average comparison between two groups, we used two-tailed Student's *t* test. Two-way ANOVA tests were performed to assess the effect on a dependent variable with two independent variables, e.g., time and phenotype. Significant differences in the mean were claimed when $P < 0.05$, with four degrees of significance ($*P < 0.05$, $**P < 0.01$, $***P < 0.001$, and $****P < 1 \times 10^{-4}$).

DATA AVAILABILITY

The RNA-sequencing data have been deposited in the GSA database (accession number HRA000978) and are available at the AlzData webserver (<http://www.alzdata.org/file/ACAA1.RNaseq.tar.gz>).

ACKNOWLEDGEMENTS

We thank Dr. Ian Logan for helpful comments and language editing. The study was supported by the National Natural Science Foundation of China (31730037 to Y.-G.Y., 31900737 to R.L., 82022017 to D.-F.Z.), the Strategic Priority Research Program (B) of CAS (XDB02020003 to Y.-G.Y.), the Bureau of Frontier Sciences and Education, CAS (grant no. QYZDJ-SSW-SMC005 to Y.-G.Y.), the Original Innovation Project "from 0 to 1" of Basic Frontier Scientific Research Program, CAS (ZDBS-LY-SM031 to R.L.), the Yunnan Science and Technology Plan Project (202001AT070107 to R.L.), the CAS "Light of West China" Program (2020000023 to R.L.), the Youth Innovation Promotion Association of CAS (to R.L. and D.-F.Z.), and the Training of High-Level Health Technical Personnel in Yunnan Province, Medical Academic Leader (D-2018047 to H.-Y.J.).

AUTHOR CONTRIBUTIONS

Y.-G.Y. and R.L. conceived and designed the experiments. R.L., Y.F., J.Y., D.-F.Z., X.L., R.B., M.X., Y.L. and X.R. performed the experiments and analyzed the data. M.Y. analyzed the RNA-seq data. L.-X.Y. identified the mouse genotype. H.-Y.J., L.T. and C.Z. provided the blood sample of patients. K.G. helped with the immunostaining assay. N.S. performed the electrophysiological experiment. R.L., Y.-G.Y. and D.-F.Z. wrote and revised the manuscript. All authors reviewed the content and approved the final version for publication.

ADDITIONAL INFORMATION

Supplementary information The online version contains supplementary material available at <https://doi.org/10.1038/s41392-021-00748-4>.

Competing interests: The authors declare no competing interests.

REFERENCES

1. Querfurth, H. W. & LaFerla, F. M. Alzheimer's disease. *N. Engl. J. Med.* **362**, 329–344 (2010).
2. Knopman, D. S. et al. Alzheimer disease. *Nat. Rev. Dis. Prim.* **7**, 33 (2021).
3. Gatz, M. et al. Role of genes and environments for explaining Alzheimer disease. *Arch. Gen. Psychiatry* **63**, 168–174 (2006).
4. Pedersen, N. L., Gatz, M., Berg, S. & Johansson, B. How heritable is Alzheimer's disease late in life? Findings from Swedish twins. *Ann. Neurol.* **55**, 180–185 (2004).
5. Guerreiro, R., Bras, J. & Hardy, J. Snapshot: genetics of Alzheimer's disease. *Cell* **155**, 968 (2013).
6. StGeorgeHyslop, P. H. et al. The genetic-defect causing familial Alzheimers disease maps on chromosome-21. *Science* **235**, 885–890 (1987).
7. Tanzi, R. E. et al. Amyloid beta protein gene: cDNA, mRNA distribution, and genetic linkage near the Alzheimer locus. *Science* **235**, 880–884 (1987).
8. Schellenberg, G. D. et al. Linkage analysis of familial Alzheimer disease, using chromosome 21 markers. *Am. J. Hum. Genet.* **48**, 563–583 (1991).
9. Kamino, K. et al. Linkage and mutational analysis of familial Alzheimer-disease kindreds for the App gene region. *Am. J. Hum. Genet.* **51**, 998–1014 (1992).
10. Schellenberg, G. D. et al. Genetic-linkage evidence for a familial Alzheimers-disease locus on chromosome-14. *Science* **258**, 668–671 (1992).
11. StGeorgeHyslop, P. et al. Genetic-evidence for a novel familial Alzheimers disease locus on chromosome-14. *Nat. Genet.* **2**, 330–334 (1992).
12. Campion, D. et al. Early-onset autosomal dominant Alzheimer disease: prevalence, genetic heterogeneity, and mutation spectrum. *Am. J. Hum. Genet.* **65**, 664–670 (1999).
13. Zhang, D. F., Xu, M., Bi, R. & Yao, Y. G. Genetic analyses of Alzheimer's disease in China: achievements and perspectives. *ACS Chem. Neurosci.* **10**, 890–901 (2019).
14. Andrews, S. J., Fulton-Howard, B. & Goate, A. Interpretation of risk loci from genome-wide association studies of Alzheimer's disease. *Lancet Neurol.* **19**, 326–335 (2020).
15. Ridge, P. G. et al. Assessment of the genetic variance of late-onset Alzheimer's disease. *Neurobiol. Aging* **41**, 200.e13–200.e20 (2016).
16. Lambert, J. C. et al. Meta-analysis of 74,046 individuals identifies 11 new susceptibility loci for Alzheimer's disease. *Nat. Genet.* **45**, 1452–1458 (2013).
17. Schwartzenuber, J. et al. Genome-wide meta-analysis, fine-mapping and integrative prioritization implicate new Alzheimer's disease risk genes. *Nat. Genet.* **53**, 392–402 (2021).
18. Ridge, P. G. E. A. Alzheimer's disease: analyzing the missing heritability. *PLoS ONE* **8**, e79771 (2013).
19. Nativio, R. et al. An integrated multi-omics approach identifies epigenetic alterations associated with Alzheimer's disease. *Nat. Genet.* **52**, 1024–1035 (2020).
20. Xiao, X., Liu, X. & Jiao, B. Epigenetics: recent advances and its role in the treatment of Alzheimer's disease. *Front. Neurol.* **11**, 538301 (2020).
21. Zhang, D. F. et al. Complement C7 is a novel risk gene for Alzheimer's disease in Han Chinese. *Natl. Sci. Rev.* **6**, 257–274 (2019).
22. Karch, C. M. & Goate, A. M. Alzheimer's disease risk genes and mechanisms of disease pathogenesis. *Biol. Psychiatry* **77**, 43–51 (2015).
23. Ghani, M., Reitz, C., George-Hyslop, P. & Rogaeve, E. Genetic complexity of early-onset Alzheimer's disease. *Neurodegener. Dis.* **2018**, 29–50 (2018).
24. Wang, J., Gu, B. J., Masters, C. L. & Wang, Y. J. A systemic view of Alzheimer disease - insights from amyloid-beta metabolism beyond the brain. *Nat. Rev. Neurol.* **13**, 612–623 (2017).
25. Butterfield, D. A. & Halliwell, B. Oxidative stress, dysfunctional glucose metabolism and Alzheimer disease. *Nat. Rev. Neurosci.* **20**, 148–160 (2019).
26. Johnson, E. C. B. et al. Large-scale proteomic analysis of Alzheimer's disease brain and cerebrospinal fluid reveals early changes in energy metabolism associated with microglia and astrocyte activation. *Nat. Med.* **26**, 769–780 (2020).
27. Toledo, J. B. et al. Metabolic network failures in Alzheimer's disease: a biochemical road map. *Alzheimers Dement.* **13**, 965–984 (2017).
28. Mahajan, U. V. et al. Dysregulation of multiple metabolic networks related to brain transmethylation and polyamine pathways in Alzheimer disease: a targeted metabolomic and transcriptomic study. *PLoS Med.* **17**, e1003012 (2020).
29. Sudmant, P. H. et al. An integrated map of structural variation in 2,504 human genomes. *Nature* **526**, 75–81 (2015).

30. Wang, G. et al. Mutation and association analyses of dementia-causal genes in Han Chinese patients with early-onset and familial Alzheimer's disease. *J. Psychiatr. Res.* **113**, 141–147 (2019).
31. Rentsch, P., Witten, D., Cooper, G. M., Shendure, J. & Kircher, M. CADD: predicting the deleteriousness of variants throughout the human genome. *Nucleic Acids Res.* **47**, D886–D894 (2019).
32. The 1000 Genomes Project Consortium. A global reference for human genetic variation. *Nature* **526**, 68–74 (2015).
33. Lek, M. et al. Analysis of protein-coding genetic variation in 60,706 humans. *Nature* **536**, 285–291 (2016).
34. Mizuno, Y. et al. Tysnd1 deficiency in mice interferes with the peroxisomal localization of PTS2 enzymes, causing lipid metabolic abnormalities and male infertility. *PLoS Genet.* **9**, e1003286 (2013).
35. Counihan, J. L. et al. Chemoproteomic profiling of acetanilide herbicides reveals their role in inhibiting fatty acid oxidation. *ACS Chem. Biol.* **12**, 635–642 (2017).
36. Zhang, D. F. et al. CFH variants affect structural and functional brain changes and genetic risk of Alzheimer's disease. *Neuropsychopharmacology* **41**, 1034–1045 (2016).
37. Xiang, Q. et al. Rare genetic variants of the Transthyretin gene are associated with Alzheimer's disease in Han Chinese. *Mol. Neurobiol.* **54**, 5192–5200 (2017).
38. Kanehisa, M., Furumichi, M., Tanabe, M., Sato, Y. & Morishima, K. KEGG: new perspectives on genomes, pathways, diseases and drugs. *Nucleic Acids Res.* **45**, D353–D361 (2017).
39. The Gene Ontology Consortium. The Gene Ontology Resource: 20 years and still GOing strong. *Nucleic Acids Res.* **47**, D330–D338 (2019).
40. Subramanian, A. et al. Gene set enrichment analysis: a knowledge-based approach for interpreting genome-wide expression profiles. *Proc. Natl Acad. Sci. USA* **102**, 15545–15550 (2005).
41. Xu, M. et al. A systematic integrated analysis of brain expression profiles reveals YAP1 and other prioritized hub genes as important upstream regulators in Alzheimer's disease. *Alzheimers Dement.* **14**, 215–229 (2018).
42. Farrer, L. A. et al. Effects of age, sex, and ethnicity on the association between apolipoprotein E genotype and Alzheimer disease - a meta-analysis. *JAMA* **278**, 1349–1356 (1997).
43. Genin, E. et al. APOE and Alzheimer disease: a major gene with semi-dominant inheritance. *Mol. Psychiatry* **16**, 903–907 (2011).
44. Bras, J. et al. Exome sequencing in a consanguineous family clinically diagnosed with early-onset Alzheimer's disease identifies a homozygous CTSF mutation. *Neurobiol. Aging* **46**, 236.e1–236.e6 (2016).
45. Sweet, R. A. et al. Catechol-O-methyltransferase haplotypes are associated with psychosis in Alzheimer disease. *Mol. Psychiatry* **10**, 1026–1036 (2005).
46. Lee, J. H. et al. Lysosomal proteolysis and autophagy require presenilin 1 and are disrupted by Alzheimer-related PS1 mutations. *Cell* **141**, 1146–1158 (2010).
47. Jankowsky, J. L. et al. Mutant presenilins specifically elevate the levels of the 42 residue beta-amyloid peptide in vivo: evidence for augmentation of a 42-specific gamma secretase. *Hum. Mol. Genet.* **13**, 159–170 (2004).
48. Kaplitt, M. G. et al. Long-term gene-expression and phenotypic correction using adenoassociated virus vectors in the mammalian brain. *Nat. Genet.* **8**, 148–154 (1994).
49. Marks, W. J. Jr. et al. Gene delivery of AAV2-neurturin for Parkinson's disease: a double-blind, randomised, controlled trial. *Lancet Neurol.* **9**, 1164–1172 (2010).
50. Wu, S. H. et al. Comparative study of the transfection efficiency of commonly used viral vectors in rhesus monkey (*Macaca mulatta*) brains. *Zool. Res.* **38**, 88–95 (2017).
51. Hijazi, S. et al. Early restoration of parvalbumin interneuron activity prevents memory loss and network hyperexcitability in a mouse model of Alzheimer's disease. *Mol. Psychiatry* **25**, 3380–3398 (2020).
52. Xiong, H. et al. Biochemical and behavioral characterization of the double transgenic mouse model (APP^{swe}/PS1^{dE9}) of Alzheimer's disease. *Neurosci. Bull.* **27**, 221–232 (2011).
53. Fu, A. K. Y. et al. IL-33 ameliorates Alzheimer's disease-like pathology and cognitive decline. *Proc. Natl Acad. Sci. USA* **113**, E2705–E2713 (2016).
54. Luo, R. et al. Activation of PPARA-mediated autophagy reduces Alzheimer disease-like pathology and cognitive decline in a murine model. *Autophagy* **16**, 52–69 (2020).
55. Alves, S. et al. Interleukin-2 improves amyloid pathology, synaptic failure and memory in Alzheimer's disease mice. *Brain* **140**, 826–842 (2017).
56. Mucke, L. & Selkoe, D. J. Neurotoxicity of amyloid beta-protein: synaptic and network dysfunction. *Cold Spring Harb. Perspect. Med.* **2**, a006338 (2012).
57. Lee, S., Sato, Y. & Nixon, R. A. Lysosomal proteolysis inhibition selectively disrupts axonal transport of degradative organelles and causes an Alzheimer's-like axonal dystrophy. *J. Neurosci.* **31**, 7817–7830 (2011).
58. Boland, B. et al. Autophagy induction and autophagosome clearance in neurons: relationship to autophagic pathology in Alzheimer's disease. *J. Neurosci.* **28**, 6926–6937 (2008).
59. Di Meco, A., Curtis, M. E., Lauretti, E. & Pratico, D. Autophagy dysfunction in Alzheimer's disease: mechanistic insights and new therapeutic opportunities. *Biol. Psychiatry* **87**, 797–807 (2020).
60. Rubinsztein, D. C. et al. In search of an "autophagometer". *Autophagy* **5**, 585–589 (2009).
61. Klionsky, D. J. et al. Guidelines for the use and interpretation of assays for monitoring autophagy (4th edition). *Autophagy* **17**, 1–382 (2021).
62. Sheng, N., Shi, Y. S. & Nicoll, R. A. Amino-terminal domains of kainate receptors determine the differential dependence on Neto auxiliary subunits for trafficking. *Proc. Natl Acad. Sci. USA* **114**, 11559–1164 (2017).
63. Tsui-Pierchala, B. A., Encinas, M., Milbrandt, J. & Johnson, E. M. Jr. Lipid rafts in neuronal signaling and function. *Trends Neurosci.* **25**, 412–417 (2002).
64. Wu, X., Cai, Q., Feng, Z. & Zhang, M. Liquid-liquid phase separation in neuronal development and synaptic signaling. *Dev. Cell* **55**, 18–29 (2020).
65. Liu, L., MacKenzie, K. R., Putluri, N., Maletic-Savatic, M. & Bellen, H. J. The glianeuron lactate shuttle and elevated ROS promote lipid synthesis in neurons and lipid droplet accumulation in glia via APOE/D. *Cell Metab.* **26**, 719.e6–737.e6 (2017).
66. Liu, L. et al. Glial lipid droplets and ROS induced by mitochondrial defects promote neurodegeneration. *Cell* **160**, 177–190 (2015).
67. Wanders, R. J., Ferdinandusse, S., Brites, P. & Kemp, S. Peroxisomes, lipid metabolism and lipotoxicity. *Biochim. Biophys. Acta* **1801**, 272–280 (2010).
68. Jo, D. S., Park, N. Y. & Cho, D. H. Peroxisome quality control and dysregulated lipid metabolism in neurodegenerative diseases. *Exp. Mol. Med.* **52**, 1486–1495 (2020).
69. Kou, J. et al. Peroxisomal alterations in Alzheimer's disease. *Acta Neuropathol.* **122**, 271–283 (2011).
70. Cipolla, C. M. & Lodhi, I. J. Peroxisomal dysfunction in age-related diseases. *Trends Endocrinol. Metab.* **28**, 297–308 (2017).
71. Mast, F. D. et al. A Drosophila model for the Zellweger spectrum of peroxisome biogenesis disorders. *Dis. Model. Mech.* **4**, 659–672 (2011).
72. Wangler, M. F. et al. Peroxisomal biogenesis is genetically and biochemically linked to carbohydrate metabolism in Drosophila and mouse. *PLoS Genet.* **13**, e1006825 (2017).
73. Kassmann, C. M. et al. Axonal loss and neuroinflammation caused by peroxisome-deficient oligodendrocytes. *Nat. Genet.* **39**, 969–976 (2007).
74. Böttelbergs, A. et al. Axonal integrity in the absence of functional peroxisomes from projection neurons and astrocytes. *Glia* **58**, 1532–1543 (2010).
75. Baes, M. et al. A mouse model for Zellweger syndrome. *Nat. Genet.* **17**, 49–57 (1997).
76. Hanson, M. G., Fregoso, V. L., Vrana, J. D., Tucker, C. L. & Niswander, L. A. Peripheral nervous system defects in a mouse model for peroxisomal biogenesis disorders. *Dev. Biol.* **395**, 84–95 (2014).
77. Chung, H. L. et al. Loss- or gain-of-function mutations in ACOX1 cause axonal loss via different mechanisms. *Neuron* **106**, 589.e6–606.e6 (2020).
78. Verheijden, S. et al. Identification of a chronic non-neurodegenerative microglia activation state in a mouse model of peroxisomal beta-oxidation deficiency. *Glia* **63**, 1606–1620 (2015).
79. Pigino, G. et al. Disruption of fast axonal transport is a pathogenic mechanism for intraneuronal amyloid beta. *Proc. Natl Acad. Sci. USA* **106**, 5907–5912 (2009).
80. Stokin, G. B. et al. Axonopathy and transport deficits early in the pathogenesis of Alzheimer's disease. *Science* **307**, 1282–1288 (2005).
81. Schrader, M. & Fahimi, H. D. Peroxisomes and oxidative stress. *Biochim. Biophys. Acta* **1763**, 1755–1766 (2006).
82. Wanders, R. J. et al. Peroxisomal fatty acid alpha- and beta-oxidation in humans: enzymology, peroxisomal metabolite transporters and peroxisomal diseases. *Biochem. Soc. Trans.* **29**, 250–267 (2001).
83. Heikoop, J. C. et al. Rhizomelic chondrodysplasia punctata. Deficiency of 3-oxoacyl-coenzyme A thiolase in peroxisomes and impaired processing of the enzyme. *J. Clin. Investig.* **86**, 126–130 (1990).
84. Bout, A. et al. Characterization of the gene encoding human peroxisomal 3-oxoacyl-CoA thiolase (ACAA). No large DNA rearrangement in a thiolase-deficient patient. *Biochim. Biophys. Acta* **1090**, 43–51 (1991).
85. Goldfischer, S. et al. Pseudo-Zellweger syndrome - deficiencies in several peroxisomal oxidative activities. *J. Pediatr.* **108**, 25–32 (1986).
86. Nixon, R. A. & Yang, D. S. Autophagy failure in Alzheimer's disease—locating the primary defect. *Neurobiol. Dis.* **43**, 38–45 (2011).
87. Bonam, S. R., Wang, F. J. & Muller, S. Lysosomes as a therapeutic target. *Nat. Rev. Drug Discov.* **18**, 923–948 (2019).
88. Peric, A. & Annaert, W. Early etiology of Alzheimer's disease: tipping the balance toward autophagy or endosomal dysfunction? *Acta Neuropathol.* **129**, 363–381 (2015).
89. LeBlanc, A. C. & Goodyer, C. G. Role of endoplasmic reticulum, endosomal-lysosomal compartments, and microtubules in amyloid precursor protein metabolism of human neurons. *J. Neurochem.* **72**, 1832–1842 (1999).

90. Nabavi, S. et al. Metabotropic NMDA receptor function is required for NMDA receptor-dependent long-term depression. *Proc. Natl Acad. Sci. USA* **110**, 4027–4032 (2013).
91. Texido, L., Martin-Satue, M., Alberdi, E., Solsona, C. & Matute, C. Amyloid beta peptide oligomers directly activate NMDA receptors. *Cell Calcium* **49**, 184–190 (2011).
92. Li, L. L. et al. Unexpected heterodivalent recruitment of NOS1AP to nNOS reveals multiple sites for pharmacological intervention in neuronal disease models. *J. Neurosci.* **35**, 7349–7364 (2015).
93. Courtney, M. J., Li, L. L. & Lai, Y. Y. Mechanisms of NOS1AP action on NMDA receptor-nNOS signaling. *Front. Cell. Neurosci.* **8**, 252 (2014).
94. Simon, R. P., Swan, J. H., Griffiths, T. & Meldrum, B. S. Blockade of N-methyl-D-aspartate receptors may protect against ischemic damage in the brain. *Science* **226**, 850–852 (1984).
95. Parsons, M. P. & Raymond, L. A. Extrasynaptic NMDA receptor involvement in central nervous system disorders. *Neuron* **82**, 279–293 (2014).
96. Gunner, G. et al. Sensory lesioning induces microglial synapse elimination via ADAM10 and fractalkine signaling. *Nat. Neurosci.* **22**, 1075–1088 (2019).
97. Jack, C. R. Jr. et al. Introduction to the recommendations from the National Institute on Aging-Alzheimer's Association workgroups on diagnostic guidelines for Alzheimer's disease. *Alzheimers Dement.* **7**, 257–262 (2011).
98. Khachaturian, Z. S. Revised criteria for diagnosis of Alzheimer's disease: National Institute on Aging-Alzheimer's Association diagnostic guidelines for Alzheimer's disease. *Alzheimers Dement.* **7**, 253–256 (2011).
99. McKhann, G. et al. Clinical diagnosis of Alzheimer's disease: report of the NINCDS-ADRDA work group under the auspices of department of health and human services task force on Alzheimer's disease. *Neurology* **34**, 939–944 (1984).
100. Bi, R. et al. Mitochondrial DNA haplogroup B5 confers genetic susceptibility to Alzheimer's disease in Han Chinese. *Neurobiol. Aging* **36**, 1604 e1607–1604 e1616 (2015).
101. Tang, J. et al. Whole-genome sequencing of monozygotic twins discordant for schizophrenia indicates multiple genetic risk factors for schizophrenia. *J. Genet. Genomics* **44**, 295–306 (2017).
102. Bolger, A. M., Lohse, M. & Usadel, B. Trimmomatic: a flexible trimmer for Illumina sequence data. *Bioinformatics* **30**, 2114–2120 (2014).
103. Li, H. & Durbin, R. Fast and accurate short read alignment with Burrows-Wheeler transform. *Bioinformatics* **25**, 1754–1760 (2009).
104. DePristo, M. A. et al. A framework for variation discovery and genotyping using next-generation DNA sequencing data. *Nat. Genet.* **43**, 491–498 (2011).
105. Liu, X., Wu, C., Li, C. & Boerwinkle, E. dbNSFP v3.0: a one-stop database of functional predictions and annotations for human non-synonymous and splice site SNVs. *Hum. Mutat.* **37**, 235–241 (2015).
106. Su, L. Y. et al. Atg5- and Atg7-dependent autophagy in dopaminergic neurons regulates cellular and behavioral responses to morphine. *Autophagy* **13**, 1496–1511 (2017).
107. Xu, L. et al. Tupaia MAVS is a dual target during hepatitis C virus infection for innate immune evasion and viral replication via NF-kappaB. *J. Immunol.* **205**, 2091–2099 (2020).
108. Yao, Y. L. et al. Tupaia OASL1 promotes cellular antiviral immune responses by recruiting MDA5 to MAVS. *J. Immunol.* **205**, 3419–3428 (2020).
109. Krauthausen, M. et al. CXCR3 promotes plaque formation and behavioral deficits in an Alzheimer's disease model. *J. Clin. Investig.* **125**, 365–378 (2015).



Open Access This article is licensed under a Creative Commons Attribution 4.0 International License, which permits use, sharing, adaptation, distribution and reproduction in any medium or format, as long as you give appropriate credit to the original author(s) and the source, provide a link to the Creative Commons license, and indicate if changes were made. The images or other third party material in this article are included in the article's Creative Commons license, unless indicated otherwise in a credit line to the material. If material is not included in the article's Creative Commons license and your intended use is not permitted by statutory regulation or exceeds the permitted use, you will need to obtain permission directly from the copyright holder. To view a copy of this license, visit <http://creativecommons.org/licenses/by/4.0/>.

© The Author(s) 2021

Supplementary Materials for

A novel missense variant in ACAA1 contributes to early-onset Alzheimer's disease, impairs lysosomal function and facilitates amyloid- β pathology and cognitive decline

Rongcan Luo^{1,#,*}, Yu Fan^{1,#}, Jing Yang^{1,2}, Maosen Ye^{1,2}, Deng-Feng Zhang¹, Kun Guo³, Xiao Li^{1,2}, Rui Bi¹, Min Xu¹, Lu-Xiu Yang¹, Yu Li^{1,2}, Xiaoqian Ran^{1,2}, Hong-Yan Jiang⁴, Chen Zhang⁵, Liwen Tan⁶, Nengyin Sheng^{3,7}, Yong-Gang Yao^{1,2,8,*}

¹ Key Laboratory of Animal Models and Human Disease Mechanisms of the Chinese Academy of Sciences & Yunnan Province, and KIZ-CUHK Joint Laboratory of Bioresources and Molecular Research in Common Diseases, Kunming Institute of Zoology, Chinese Academy of Sciences, Kunming, Yunnan 650204, China

² Kunming College of Life Science, University of Chinese Academy of Sciences, Kunming, Yunnan 650204, China

³ State Key Laboratory of Genetic Resources and Evolution, Kunming Institute of Zoology, Chinese Academy of Sciences, Kunming 650201, China

⁴ Department of Psychiatry, the First Affiliated Hospital of Kunming Medical University, Kunming 650032, China

⁵ Division of Mood Disorders, Shanghai Mental Health Center, Shanghai Jiao Tong University School of Medicine, Shanghai 200030, China

⁶ Mental Health Institute of the Second Xiangya Hospital, Central South University, Changsha 410011, China

⁷ Center for Excellence in Animal Evolution and Genetics, Chinese Academy of Sciences, Kunming, Yunnan 650201, China

⁸ CAS Center for Excellence in Brain Science and Intelligence Technology, Chinese Academy of Sciences, Shanghai 200031, China

These authors contributed equally to this work

* Corresponding author, E-mail addresses: yaoyg@mail.kiz.ac.cn (Y.-G. Yao),
luorongcan@mail.kiz.ac.cn (R. Luo)

This PDF file includes:

Supplementary Materials and Methods

Figures S1 to S7

Tables S1 to S4

Supplementary Materials and Methods

Cell culture and transfection

The U251 glioma cells, human microglia (HM), SH-SY5Y neuroblastoma cells were introduced from Kunming Cell Bank, Kunming Institute of Zoology (KIZ), Chinese Academy of Sciences (CAS). We introduced human APP mutant K670N/M671L into U251 cells for stable expression (U251-APP cell), and this cell line produced A β under doxorubicin induction^{1,2}. We overexpressed ACAA1 WT and ACAA1 p.N299S in the U251-APP cells and HM cells to characterize their potential effects. Briefly, the U251-APP cells and HM cells were cultured in Roswell RPMI-1640 medium and Dulbecco's modified Eagle's medium (DMEM; Gibco-BRL, 11965-092), respectively, supplemented with 10% fetal bovine serum (FBS) (Gibco-BRL; 10099-141), 100 U/ml penicillin and 100 mg/mL streptomycin at 37°C in a humidified atmosphere incubator with 5% CO₂. Transfection of empty vector, expression vector of ACAA1 WT, and expression vector of ACAA1 p.N299S in U251-APP cells or HM cells, was performed using an electroporator (CUY21EDIT, Nepa gene Co., Japan) following the manufacturer's instructions. After cells were trypsinized and washed three times with Opti-MEM medium (Gibco-BRL), around 1×10^6 cells were resuspended in 100 μ L Opti-MEM medium, and were electroporated with 10 μ g plasmids. Transfected cells were seeded in pre-warmed growth medium for 72 h in 5% CO₂ at 37°C before the harvest.

The SH-SY5Y cells were maintained in DMEM supplemented with 10% FBS, 1 \times MEM nonessential amino acid solution (Gibco, 11140050), 100 U/ml penicillin and 100 mg/ml streptomycin at 37°C in a humidified atmosphere incubator with 5% CO₂. For knockdown of the *ACAA1* gene in this cell line, three small interfering RNAs (siRNAs: siRNA-1, 5'-GAGCAAGGGCTGTTTCCAA-3'; siRNA-2, 5'-CCGCTGCCGTCTTTGAATA-3'; siRNA-3, 5'-TGAGCGGTTTGGCATTTC-3') targeting *ACAA1* and a negative control siRNA (NC siRNA) were synthesized by RiboBio (Guangzhou, China). The SH-SY5Y cells (2×10^5 per well) were seeded in 6-well plates to grow to 50% confluence, then culture medium was removed and washed once with the Opti-MEM medium before the transfection. The *ACAA1* siRNA or NC siRNA was dissolved in the Opti-MEM medium, then was mixed with 6 μ L LipofectamineTM 3000 (Invitrogen, L3000008) to achieve a final volume of 150 μ L for forming the siRNA-Lipofectamine mixture for 20 min at room temperature. The mixture was added to each well, together with an additional 850 μ L Opti-MEM medium. After an incubation of 6 h, the medium was removed and 2 mL fresh medium was added to each well for growth. We used three siRNA concentrations (12.5 nM, 25 nM, 50 nM) to optimize the knockdown efficiency, and transfected cells were harvested at 48 h. Transfection of empty vector and expression vector of ACAA1 WT or mutant p.N299S was performed by using the LipofectamineTM 3000 with a similar procedure as for siRNA transfection.

Evolutionary conservation analysis

Evolutionary conservation analysis was performed to show the overall sequence identity of the ACAA1 protein sequences. We retrieved the ACAA1 protein sequences of 13 vertebrate species, including human (*Homo sapiens*, ID: 30), chimpanzee (*Pan troglodytes*, ID: 460268), gorilla (*Gorilla gorilla gorilla*, ID: 101141231), pig-tailed macaque (*Macaca nemestrina*, ID: 105480193), Chinese tree shrew (*Tupaia chinensis*, ID: 102470441), house mouse (*Mus musculus*, ID: 113868), norway rat (*Rattus norvegicus*, ID: 24157), pig (*Sus scrofa*, ID: 100515577), cattle (*Bos taurus*, ID: 508324), dog (*Canis lupus familiaris*, ID: 477023), domestic

cat (*felis catus*, ID: 101087343), chicken (*Gallus gallus*, ID:770094), and zebrafish (*danio rerio*, ID: 431754), from NCBI (<http://www.ncbi.nlm.nih.gov>). Protein sequence alignment was performed by ClusterW method using software MEGA 7.0³.

RNA-sequencing (RNA-seq) analysis

We followed the procedure in our previous study for the RNA-seq analysis⁴. In brief, we extracted total RNA from transfected U251-APP cells and HM cells by using the RNA isolation kit (TianGen, Co. Ltd.). We only used RNA samples with a high quality, as reflected by an A260/A280 ratio of 1.8-2.0 to construct library for RNA-seq. Sequencing libraries were generated using the NEBNextUltra™ RNA Library Prep kit for Illumina (NEB, USA) following the manufacturer's recommendation, and were sequenced on an Illumina-HiSeq 4000 platform. The raw sequencing reads (150 bp paired-ends reads) were first trimmed by Trimmomatic (version 0.38) software⁵ to remove the adapter sequences and low-quality sequences using the following parameters "LEADING:3 TRAILING:3 SLIDINGWINDOW:4:15 MINLEN:36". After reads trimming, the clean reads were aligned to the human reference genome GRCh38.p13 (https://www.ncbi.nlm.nih.gov/assembly/GCF_000001405.39) using STAR software (version 2.6.0c)⁶. Next, the aligned reads in bam format generated by STAR were subjected to featureCounts⁷ to assign and count the uniquely mapped fragments to exons according to the annotation file of GRCh38.p13. We used rlogTransformation function of R package DESeq2⁸ to normalize and scale reads counts generated in the previous step. Principal component analysis and differential expression analysis were performed using the DESeq2⁸ based on the normalized count. The *P* values were adjusted (P_{adjust}) by the Benjamini & Hochberg (BH) method. We defined differentially expressed genes (DEGs) between different conditions if $P_{\text{adjust}} < 0.05$. Gene Ontology (GO)⁹ and Kyoto Encyclopedia of Genes and Genomes (KEGG)¹⁰ pathway enrichment analyses were performed for DEGs using R package clusterProfiler¹¹. The gene set enrichment analysis (GSEA)¹² was performed based on the \log_2 fold change of DEGs obtained from differential gene analysis, and all molecular signature databases provided by MSigDB (<https://www.gsea-msigdb.org/gsea/msigdb/index.jsp>) were tested for enrichment.

Western blotting

Western blotting was performed as described in our previous studies^{13,14}. In brief, lysates of different mouse brain tissues, transfected HM cells, U251-APP cells and SH-SY5Y cells were prepared using the protein lysis buffer (Beyotime Institute of Biotechnology, P0013) with phosphatase and protease inhibitors (Abcam, ab201119). We measured protein concentration of each sample by using the BCA protein assay kit (Beyotime Institute of Biotechnology, P0012). Around 20 μg protein was separated by 12% SDS PAGE, and was transferred to a polyvinylidene difluoride membrane (Bio-Rad, L1620177 Rev D). After the membrane was soaked with 5% (w/v) skim milk for 2 h at room temperature, membrane was incubated with the respective primary antibodies overnight at 4°C. The membrane was washed 3 times with Tris-buffered saline with 0.1% Tween 20 (TBST), each time 5 min, followed by incubation with the peroxidase-conjugated anti-mouse or anti-rabbit IgG (1:10000; KPL) for 1 h at room temperature. The membrane was visualized using an ECL Western blot detection kit (Millipore, WBKLS0500). ImageJ (National Institutes of Health, Bethesda, Maryland, USA) was used to evaluate the densitometry. Western blot for ACTB, β -tubulin, or GAPDH was used as a loading control.

Electrophysiology in slice cultures

The electrophysiology in brain slice cultures was performed following the previously described protocol^{15,16}. Briefly, organotypic rat hippocampal slice cultures were made from postnatal day 6-8 (P6-P8) rat. The ACAA1 WT and ACAA1 p.N299S were subcloned into the pCAGGS vector harboring EGFP. Biolistic transfections were performed on day in vitro (DIV) 2 after culture using a Helios Gene Gun (Bio-Rad) with 1 μ m DNA-coated gold particles. Slices were maintained at 34 °C with medium changes every other day. On DIV 8, voltage-clamp dual whole-cell recordings for CA1 pyramidal neurons were taken from a fluorescent transfected neuron and a neighboring un-transfected control neuron. During recording, slices were transferred to a perfusion stage on an Olympus BX51WI upright microscope and perfused at 2.5 mL/min with artificial cerebrospinal fluid (ACSF: 119 mM NaCl, 2.5 mM KCl, 4 mM CaCl₂, 4 mM MgSO₄, 1 mM NaH₂PO₄, 26.2 mM NaHCO₃, and 11 mM glucose) bubbled with 95% O₂ and 5% CO₂. Series resistance was monitored on-line. We discarded recordings in these series increased to >30 MOhm or varied by >50% between neurons. Dual whole-cell recordings measuring evoked excitatory postsynaptic currents (EPSCs) were performed. When measuring EPSCs, 100 μ M picrotoxin was added to block inhibitory currents and 4 μ M 2-Chloroadenosine was used to control epileptiform activity. Internal solution was composed of 135 mM CsMeSO₄, 8 mM NaCl, 10 mM HEPES, 0.3 mM EGTA, 5 mM QX314-Cl, 4 mM MgATP, 0.3 mM Na₃GTP, and 0.1 mM spermine. A bipolar stimulation electrode was placed in stratum radiatum, and responses were evoked at 0.2 Hz. Peak AMPAR responses were recorded at -70 mV, and NMDAR responses were recorded at +40 mV, with amplitudes measured 100 ms after stimulation to avoid contamination by AMPAR current. Paired-pulse ratio was determined by delivering two stimuli 40 ms apart and dividing the peak response to stimulus 2 by the peak response to stimulus 1. Peak GABA currents were recorded at 0 mV. All the data were analyzed off-line with custom software (IGOR Pro). Responses were collected with a Multiclamp 700A amplifier (Axon Instruments), filtered at 2 kHz, and digitized at 10 kHz.

Behavioral tests

The locomotor activity of mice in the open-field test were recorded and tracked using the SMART 3.0 software (Panlab HARVARD, MA, USA), as previously described¹⁷ with slight modifications. In brief, mice were individually placed in the center of an open-top chamber (40 × 40 × 40 inches) with an array of photobeams around the periphery, and allowed to explore the chamber for 15 min each day for 3 consecutive days. Locomotor activity in the three training trials was recorded by the photobeams, and the distance moved was recorded. We cleaned the chamber with 70% ethanol after each trial.

The contextual fear conditioning behavioral assessment was performed as previously described¹⁷. On the 1st day of training, mice were allowed to explore in an enclosed training chamber with the floor wired to an electric shock generator for 180 s. The animals were then exposed to a pure tone for 30 s, followed by a 2-s foot shock (0.8 mA). At 60 s after delivery of the shock, mice were returned to their home cages. The fear response (freezing) was assessed at the 1st day and the 7th day after the electric shock. Mice were re-exposed in the original chamber for 8 min (context test), and the time of freezing was measured using the Ugo Basile Fear Conditioning System (UGO).

Morris water maze behavioral assessment was performed as previously described^{13,18}. Briefly, experiments were performed in a 120-cm diameter, 50-cm deep tank filled with

opacified water at $20 \pm 1^\circ\text{C}$. The tank was equipped with a 10-cm diameter platform submerged 1 cm under the water surface. Training course contained daily sessions (3 trials per session) for 7 consecutive days. The start positions varied pseudorandomly among the 4 cardinal points. Mean intertrial interval was 90 min. We ended each trial when the animal reached the platform. A 60 sec cut-off was used, after which mice were gently guided to the platform. Once on the platform, animals were given a rest for 20 s before being returned to their cage. Four h (short-term memory) and 72 h after the last training trial (day 10), retention was assessed during probe trial in which the platform was removed. Animals were video-tracked using SMART 3.0 software (Panlab HARVARD, MA, USA). Behavioral parameters, including swim speed, travelled distance, latency, percentage of time in each quadrant, percentage of distance in each quadrant, were automatically calculated. For all behavioral tests, the experimenter was blinded to the genotypes of mice.

Brain dissection, immunohistochemistry, and immunofluorescence

The APP/PS1 ΔE9 mice and WT littermates with AAV-mediated gene delivery were sacrificed at 6 months post-injection. Following anesthesia, mice were transcardially perfused with ice-cold 0.1 M PBS (pH 7.4) before dissection. The left cerebral hemisphere was dissected and post-fixed in 4 % PFA for 1 week, followed by embedded in paraffin wax for immunohistochemistry analysis or in optimal cutting temperature (OCT) compound for immunohistochemistry and immunofluorescence assays. The paraffin-embedded brain slices (4 μm thickness) were cut using a microtome (Leica, Germany) and stored at room temperature. The OCT-embedded brain slices (at 10 μm thickness) were cut using a freezing microtome (Leica, Germany) and stored at -80°C . Each brain slice of APP/PS1 ΔE9 mice was incubated with mouse anti- β -amyloid (antibody 4G8; 1:500; BioLegend, 800701) overnight at 4°C . After 3 washes with PBS, the brain slice was incubated with horseradish peroxidase-labeled goat anti-mouse (1:200; Servicebio, GB23301) for 1 h at room temperature. Images were acquired by scanning with the Panoramic Digital Slide Scanner (3DHISTECH) and were processed with CaseViewer software (3DHISTECH). The staining intensity was quantified by using ImageJ software (National Institutes of Health, Bethesda, Maryland, USA).

We followed the previously reported protocol for immunofluorescence assays^{13,14}. In brief, after antigen retrieval, brain sections were blocked in PBS supplemented with 5% BSA for 1 h. Sections were then incubated with the respective primary antibodies (**Table S4**) overnight at 4°C . After washing with PBS, sections were incubated with the respective secondary antibodies (**Table S4**). The sections were then subjected to DAPI staining (1:1000; Invitrogen, D1306) for 15 min, before being sealed with antifade mounting medium (Beyotime Institute of Biotechnology, P0128M) and glass covers. Images were acquired using the same procedure and scanner as above. Counts of NeuN-positive cells were assessed for the degree of neuronal loss in the hippocampal CA3 region. Quantification of the number and area of A β plaques was performed using the particle analysis tool of the ImageJ software as previously described¹⁹.

ELISA for A β

We followed the previously reported protocols to isolate plaque-related insoluble and soluble A β ^{13,20}. In brief, hippocampus and cortex tissues from APP/PS1 ΔE9 mice were stored at -80°C after collection. Upon use, each sample was homogenized with 300 μL of RIPA lysis buffer (Beyotime Institute of Biotechnology, P0013) containing protease and phosphatase inhibitors (Abcam, ab201119) on ice, followed by centrifugation at 13,000 g for 15 min at 4°C to collect

supernatants and pellets, respectively. The protein concentrations of the supernatants were measured by using BCA protein assay kit and were adjusted to same concentration for quantifying soluble A β by ELISA. The pellets were resuspended in a volume of 300 μ L of RIPA lysis buffer, followed by centrifugation at 13,000g for 15 min at 4°C to remove potential soluble A β . This washing step was repeated 3 times to remove all soluble A β . Then, the pellets containing insoluble A β were solubilized in sodium dodecyl sulfate (SDS) buffer (2% SDS, 25 mM Tris-HCl, pH 7.4)^{13,20}. After pulsed sonication for 15 sec, the SDS fractions were quantified for protein concentrations and processed for measuring insoluble A β , using the same procedure for soluble A β . The levels of A β 40/A β 1-40 and A β 42/A β 1-42 in mouse brain tissues and U251-APP cell culture supernatant were determined by using A β 40 kit (Elabscience, E-EL-H0542c) and A β 42 kit (Elabscience, E-EL-H0543c), respectively.

rs117916664 (p.N299S)

	
AD patient	LGGAVALGHPLGCTGARQVITLLSELKRRGKRAYGVVSMC
Human	LGGAVALGHPLGCTGARQVITLLNELKRRGKRAYGVVSMC
Chimpanzee	LGGAVALGHPLGCTGARQVITLLNELKRRGKRAYGVVSMC
Gorilla	LGGAVALGHPLGCTGARQVITLLNELKRRGKRAYGVVSMC
Macaque	LGGAVALGHPLGCTGARQVITLLNELKRRGKRAYGVVSMC
Tree shrew	LGGAVALGHPLGCTGARQVVTLLNELKRRGRRAYGVVSMC
Mouse	LGGAIALGHPLGCTGARQVVTLLNELKRRGRRAYGVVSMC
Rat	LGGAIALGHPLGCTGARQVVTLLNELKRRGRRAYGVVSMC
Pig	LGGAVALGHPLGCTGARQVITLLNELKRRGKRAYGVVSMC
Cattle	LGGAVALGHPLGCTGARQVITLLNELKRRGKRAYGVVSMC
Dog	LGGAVALGHPLGCTGARQVITLLNELKRRGKRAYGVVSMC
Cat	LGGAVALGHPLGCTGARQVITLLNELKRRGKRAYGVVSMC
Chicken	LGGAIALGHPLGCTGARQVVTLLNELKRRGKRAYGVVSMC
Zebrafish	NGGAIAFGHPLGCTGARQVVTLLNELKRRRKRFGVVSMC

Figure S1. Evolutionary conservation of ACAA1 p.N299S. Alignment of ACAA1 protein sequences from different species. The ACAA1 protein sequences of human (*Homo sapiens*, ID: 30), chimpanzee (*Pan troglodytes*, ID: 460268), gorilla (*Gorilla gorilla gorilla*, ID: 101141231), pig-tailed macaque (*Macaca nemestrina*, ID: 105480193), Chinese tree shrew (*Tupaia chinensis*, ID: 102470441), house mouse (*Mus musculus*, ID: 113868), rat (*Rattus norvegicus*, ID: 24157), pig (*Sus scrofa*, ID: 100515577), cattle (*Bos taurus*, ID: 508324), dog (*Canis lupus familiaris*, ID: 477023), cat (*Felis catus*, ID: 101087343), chicken (*Gallus gallus*, ID: 770094), and zebrafish (*Danio rerio*, ID: 431754), were from NCBI (<http://www.ncbi.nlm.nih.gov>).

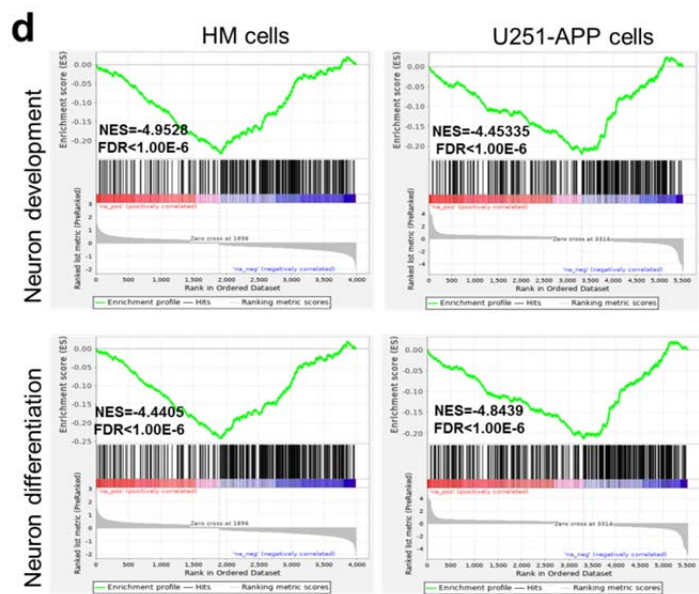
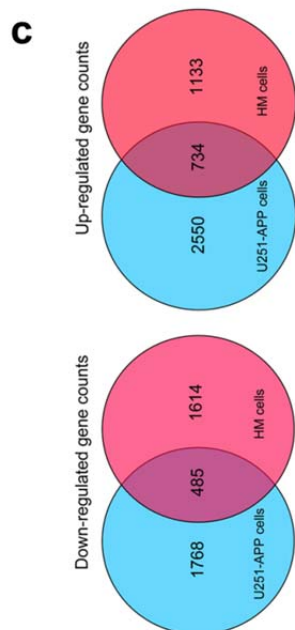
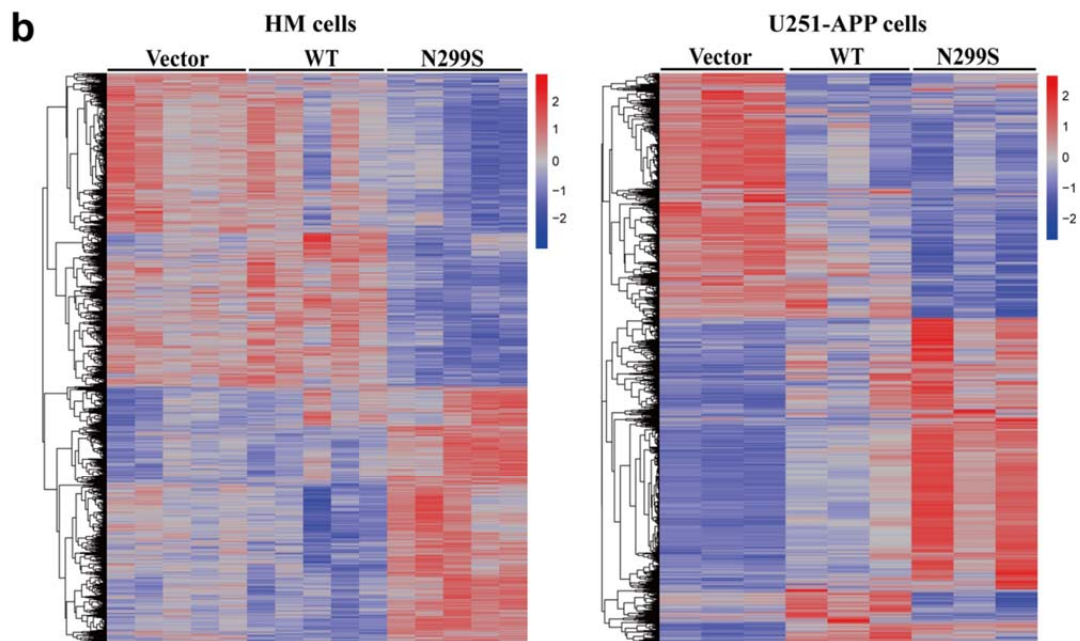
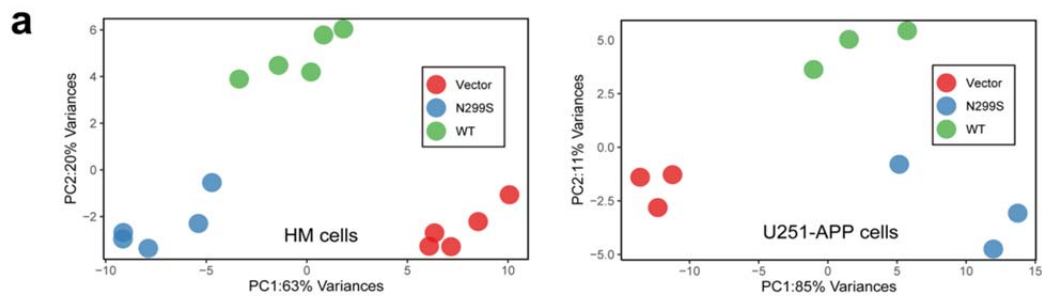


Figure S2. RNA-seq analyses of U251-APP and HM cells with overexpression of ACAA1 WT and ACAA1 p.N299S. (a) Principal component analysis (PCA) of U251-APP and HM cells with overexpression of wild type ACAA1 (WT) and ACAA1 p.N299S (N299S), as well as the empty vector (Vector). PCA was performed based on the expression values of all expressed genes, and each point represented a sample. (b) Expression heatmaps of HM cells (*Left*) and U251-APP cells (*right*) with overexpression of wild type ACAA1 (WT), ACAA1 p.N299S (N299S), and the empty vector (Vector). (c) Venn diagram of differentially expressed genes (DEGs) identified in U251-APP and HM cells with overexpression of ACAA1 WT and ACAA1 N299S. (d) Gene set enrichment analyses (GSEA) showed the enrichment of neuron development and neuron differentiation in in HM (*left panel*) and U251-APP (*right panel*) cells. NES, normalized enrichment score; FDR, false discovery rate.

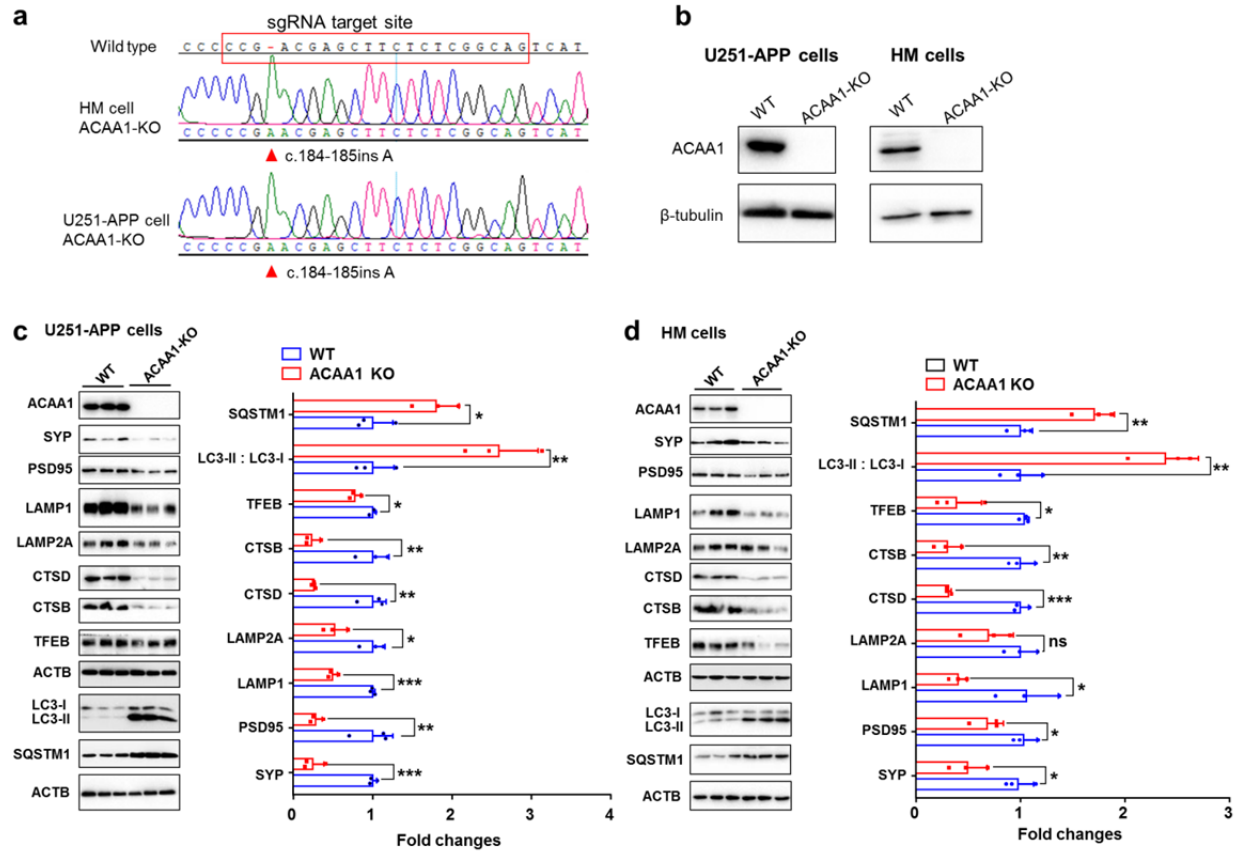


Figure S3. Knockout of ACAA1 in U251-APP and HM cells impaired levels of lysosomal and postsynaptic proteins and affected autophagy. Successful knockout of the *ACAA1* gene in HM cells and U251-APP cells by using the CRISPR/Cas9 technology (a-b). (a) Sequencing chromatographs showing the introduced mutations in the *ACAA1* gene in U251-APP and HM cells with successful gene editing (ACAA1-KO) and the unedited cells (WT). (b) Absence of the ACAA1 protein in these ACAA1-KO cells. The β -tubulin was used as the loading control. (c-d) ACAA1 knockout caused decreased levels of LAMP1, LAMP2A, CTSD, CTSB, TFEB, SYP and PSD95, but increased LC3-II:LC3-I ratio and SQSTM1 protein level in U251-APP (c) and HM (d) cells. The ACTB was used as the loading control. Data are representative of 3 independent experiments with similar results. ns, not significant; *, $P < 0.05$; **, $P < 0.01$; ***, $P < 0.001$; Students t test. Bars represent mean \pm SD of the three experiments.

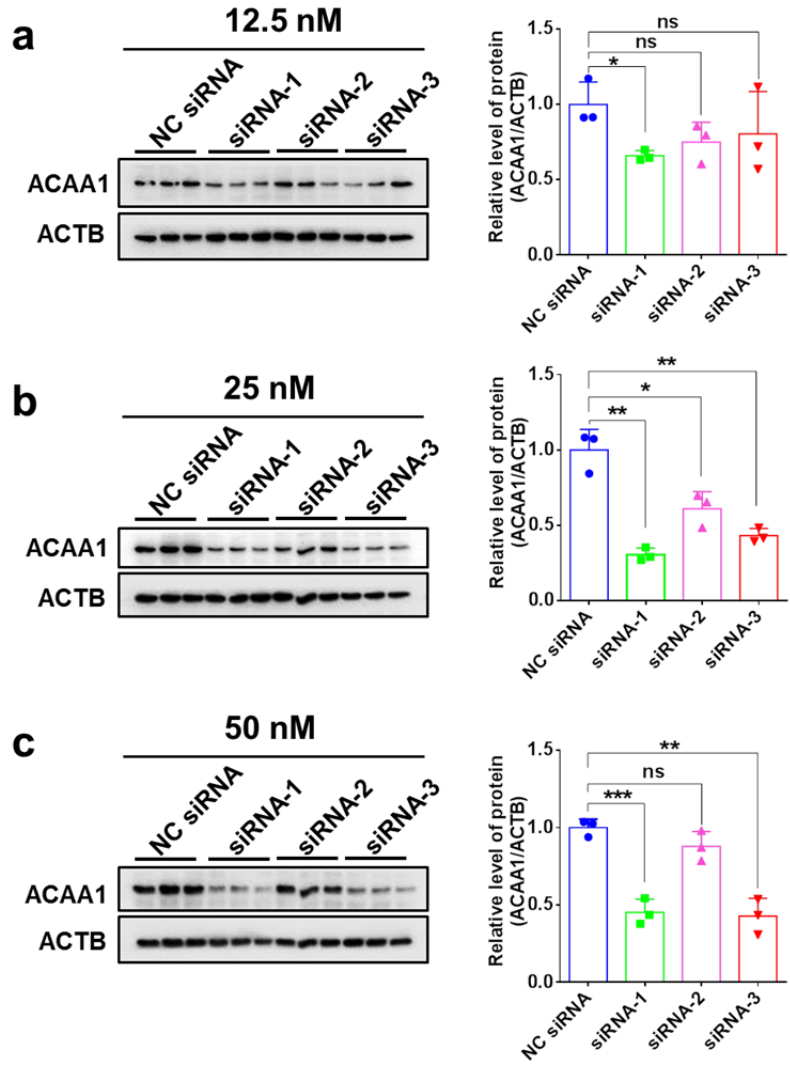


Figure S4. Knockdown efficiency of the *ACAA1* siRNAs in human SH-SY5Y cells. Cells were transfected with each of 3 *ACAA1* siRNAs (siRNA-1, siRNA-2 and siRNA-3) and negative control siRNA (NC siRNA), respectively, for 48 h before harvest for Western blotting analysis. The siRNAs were used at different concentrations of 12.5 nM (a), 25 nM (b) and 50 nM (c). Each transfection contains 3 wells in a 6-well plate. Relative protein abundance was normalized to the ACTB. ns, not significant; *, $P < 0.05$; **, $P < 0.01$; Student's t test. Bars represent mean \pm SD.

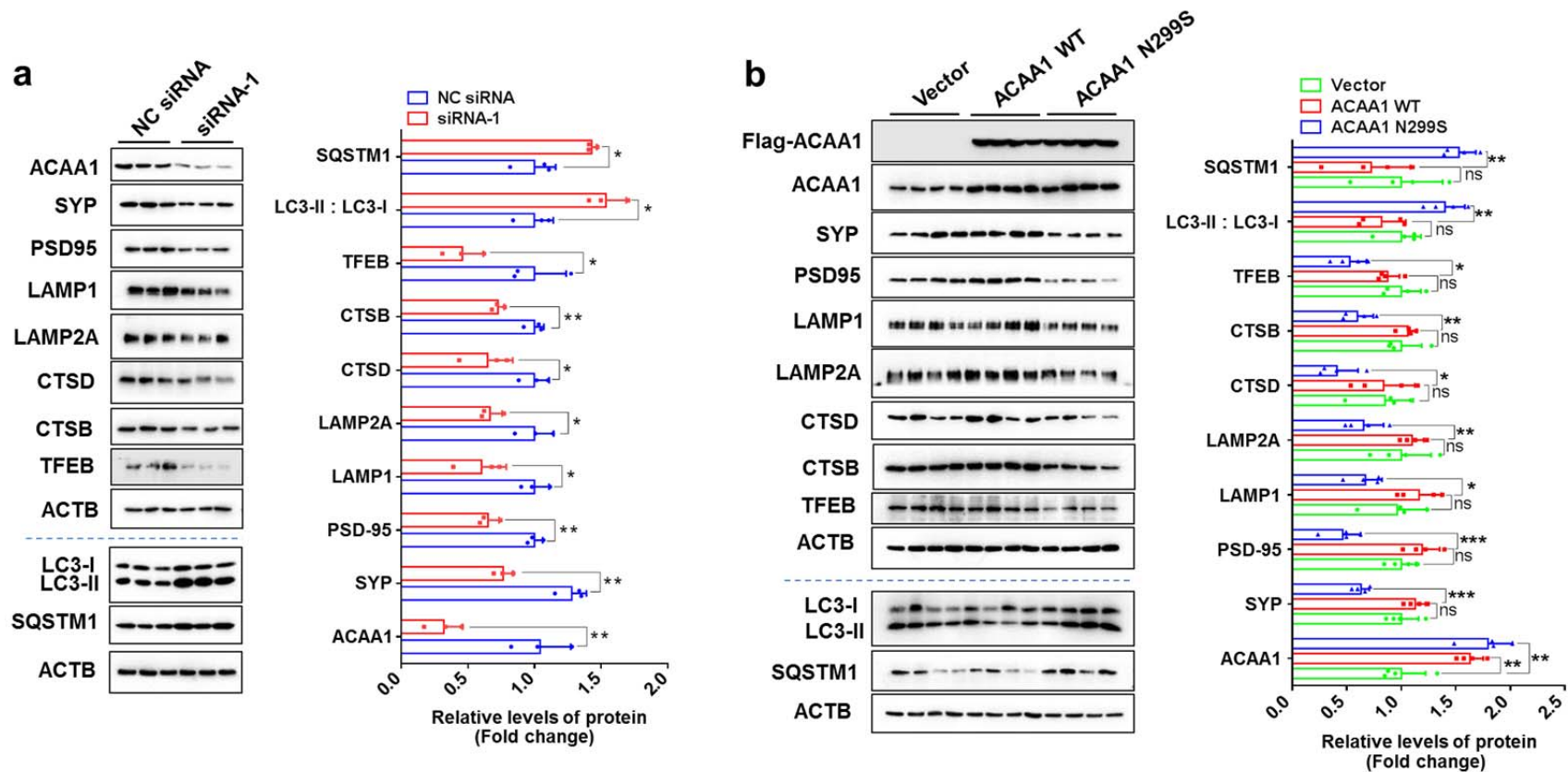


Figure S5. Knockdown of the *ACAA1* gene or overexpression of *ACAA1* p.N299S disturbed the lysosomal and synaptic functions and declined autophagy in SH-SY5Y cells.

(a-b) *ACAA1* knockdown (a) and overexpression of *ACAA1* p.N299S (b) caused decreased lysosomal protein levels of LAMP1, LAMP2A, CTSD, CTSB, TFEB, SYP and PSD95, but increased LC3-II:LC3-I ratio and SQSTM1 level in SH-SY5Y cells. The ACTB was used as the loading control. Data are representative of 3 independent experiments with similar results. ns, not significant; *, $P < 0.05$; **, $P < 0.01$; ***, $P < 0.001$; Students *t* test. Bars represent mean \pm SD of the three experiments.

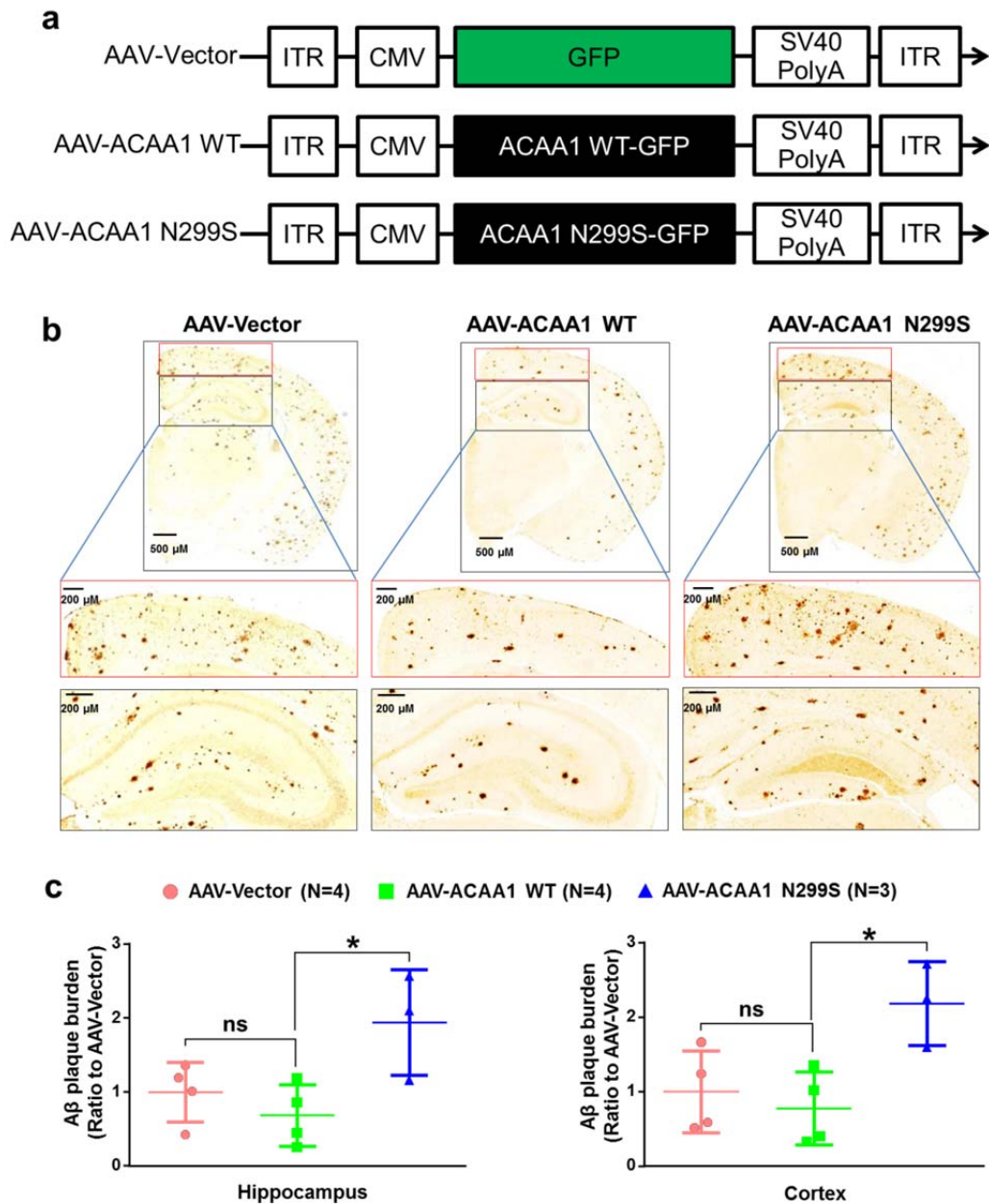


Figure S6. Administration of ACAA1 p.N299S increased amyloid plaque burden in APP/PS1ΔE9 mice.

(a) A schematic representation of the AAV vector system. The AAV php.eb-CMV-GFP constructs enabling the broad-spectrum expression of GFP (AAV-Vector), GFP-tagged ACAA1 WT (AAV-ACAA1 WT) and ACAA1 p.N299S (AAV-ACAA1 N299S) were constructed. ITR: inverted terminal repeat; GFP: GFP-tag; SV40 PolyA: SV40 poly A signal addition functions to terminate transcription from upstream promoter activity. (b-c) Overexpression of ACAA1 p.N299S aggravated amyloid plaque pathology in APP/PS1ΔE9 mice. Representative immunohistochemistry images (b) and quantification of 4G8-stained amyloid plaques in the hippocampus and cortex tissues (c) of APP/PS1ΔE9 mice after delivery of AAV-Vector, AAV-ACAA1 WT and AAV-ACAA1 N299S. N = 4 or 3 mice per group. ns, not significant; * $P < 0.05$, Student's t test. Bars represent mean \pm SD.

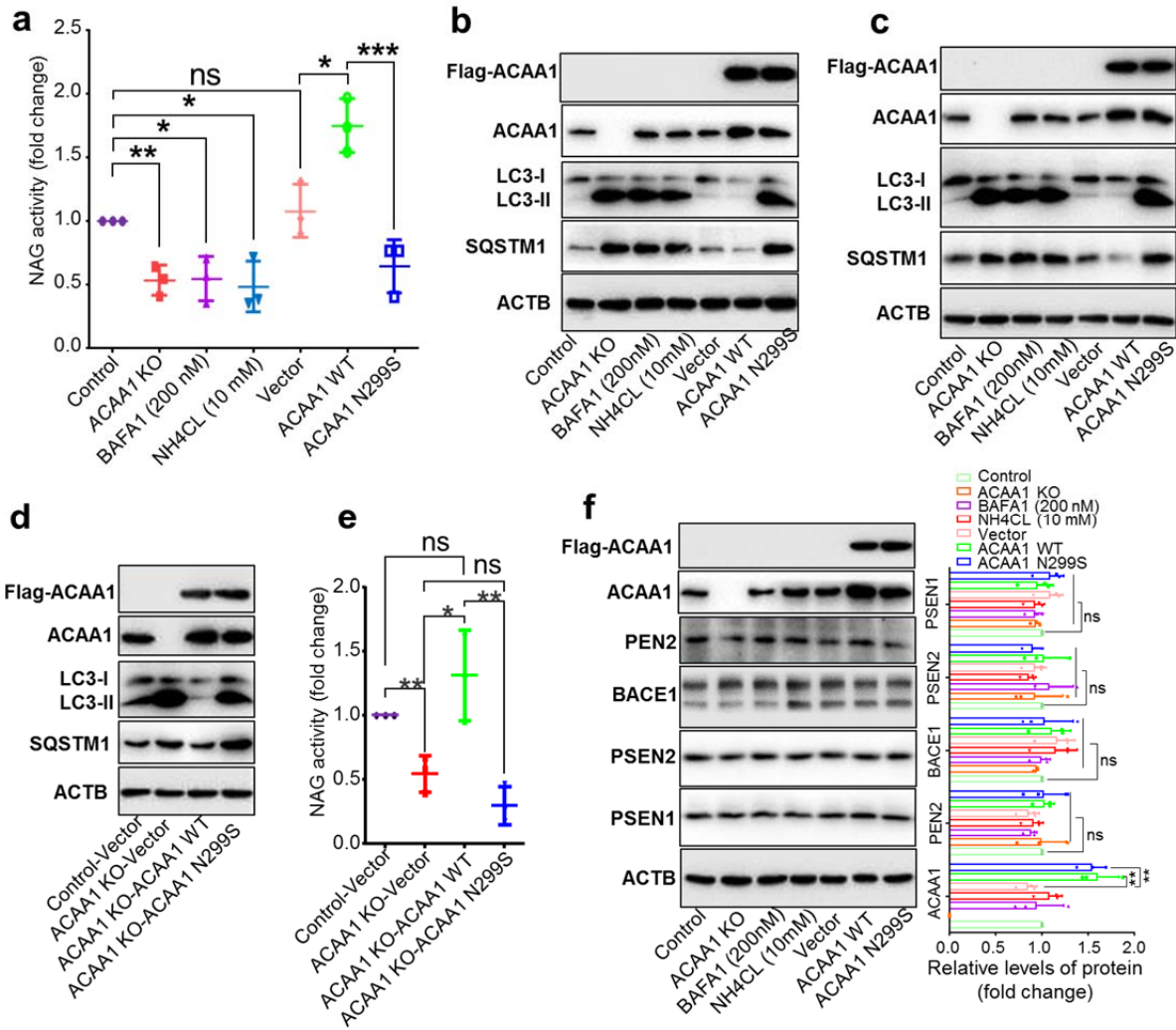


Figure S7. ACAA1 p.N299S impaired autophagy and lysosomal function in U251-APP and HM cells. (a) Knockout of ACAA1 or overexpression of ACAA1 p.N299S in HM cells led to a reduction of NAG activity, similar to the inhibition effect of BAFA1 and NH4CL treatments. (b-c) Knockout of ACAA1 or overexpression of ACAA1 p.N299S affected autophagy in U251-APP cells (b) and HM cells (c), similar to that of BAFA1 and NH4CL treatments. (d-e) Overexpression of ACAA1 WT, but not ACAA1 p.N299S, rescued the altered autophagy (d) and lysosomal activity (e) in HM ACAA1 KO cells. (f) Knockout of ACAA1 or overexpression of ACAA1 p.N299S had no effect on the protein levels of BACE1, PSEN1, PSEN2 and PEN2 in U251-APP cells. Control, cells without ACAA1 knockout. For chemical treatments, cells treated with BAFA1 at a concentration of 200 nM or NH4CL at a concentration of 10 mM. For transfection, cells were transfected with empty vector (Vector) or expression vectors for ACAA1 WT and ACAA1 p.N299S, respectively. Shown data were representative of three independent experiments. ns, not significant; *, $P < 0.05$; **, $P < 0.01$; ***, $P < 0.001$; Student's t test. Bars represent mean \pm SD.

Table S1.

Rare damaging missense variants in known dementia-causal genes in four individuals of the EOFAD family

Causal genes	Gene	Chr	Position	SNP_ID	Frequency (1000 Genomes)	Ref	Function	Individuals				Damaging Prediction
								EADQ01 (II:1)	EADM02 (III:4)	EADS03 (II:3, AD)	EADX04 (III:3)	
Alzheimer disease	<i>APP</i>	-	-	-	-	-	-	-	-	-	-	-
	<i>PSENI</i>	-	-	-	-	-	-	-	-	-	-	-
	<i>PSEN2</i>	chr1	227075798	.	NA	C	p.H169N	C/C	C/A	C/C	C/C	0
	<i>UNC5C</i>	chr4	96106322	rs2289043	0.495	A	p.M721T	G/G	G/G	A/G	G/G	2
Dementia with Lewy bodies	<i>LRRK2</i>	chr12	40713901	rs11564148	0.286	T	p.S1647T	T/A	T/A	T/A	T/T	0
	<i>LRRK2</i>	chr12	40619082	rs2256408	0.969	G	p.R50H	A/A	A/A	A/A	A/A	0
	<i>LRRK2</i>	chr12	40677699	rs34410987	0.002	C	p.P755L	C/C	C/C	C/C	C/T	0
	<i>LRRK2</i>	chr12	40657700	rs7308720	0.099	C	p.N551K	C/G	C/C	C/C	C/C	3
	<i>LRRK2</i>	chr12	40758652	rs3761863	0.552	T	p.M2397T	C/C	T/C	T/C	T/T	0
	<i>PINK1</i>	chr1	20977000	rs1043424	0.301	A	p.N521T	A/A	A/A	A/C	A/C	0
	<i>PINK1</i>	chr1	20972111	rs3738136	0.123	G	p.A340T	G/G	G/G	G/G	G/A	0
Vascular dementia	<i>COLAA1</i>	chr13	110839550	rs536174	1.000	T	p.T555P	G/G	G/G	G/G	G/G	0
	<i>COLAA1</i>	chr13	110959356	rs9515185	0.424	C	p.V7L	C/G	G/G	C/G	C/G	0
	<i>COLAA1</i>	chr13	110818598	rs3742207	0.288	T	p.Q1334H	T/T	T/T	T/G	T/G	0
	<i>NOTCH3</i>	chr19	15271771	rs1044009	0.629	G	p.A2223V	A/A	A/A	A/A	G/A	0
Other neurodegenerative disorders	<i>DNMT1</i>	chr19	10291113	rs75616428	0.008	C	p.V120L	C/C	C/C	C/C	C/G	0
	<i>DNMT1</i>	chr19	10273372	rs2228612	0.198	T	p.I311V	T/C	T/C	T/C	C/C	0
	<i>DNMT1</i>	chr19	10291181	rs16999593	0.045	T	p.H97R	T/C	T/C	T/C	T/C	0
	<i>CSF1R</i>	chr5	149450132	rs10079250	0.153	T	p.H362R	T/C	T/C	C/C	T/C	1

Causal genes were defined as described in our previous study²¹. We detected all the rare (MAF \leq 0.01 in the dataset if the 1000 Genomes Project^{22,23}), inherited loss-of-function (i.e. stop-gain or frameshift) and damaging missense variants in the four individuals underwent whole genome sequencing. Damaging prediction was scored by the number of prediction algorithms (SIFT²⁴, PolyPhen2 HumDiv, PolyPhen2 HumVar^{25,26}, LRT²⁷ and MutationTaster²⁸) by which the variant was predicted to be damaging. Missense variants were rated as damaging when at least two of the five predictions suggested a potential deleterious effect. “0” means none of the five prediction algorithms suggesting a damaging effect. There are no rare or damaging variants in the *APP* and *PSENI* genes in the four individuals, and was marked with “-“.

Chr, chromosome; Position, physical position of the variant; SNP_ID, rsID in dbSNP (<https://www.ncbi.nlm.nih.gov/snp/>); Ref, reference allele, allele of reference genome hg19 (also known as GRCh37, https://grch37.ensembl.org/Homo_sapiens).

Table S2.**Validation of the rare damaging variants in the EOFAD family using whole-exome data of Chinese patients with EOFAD**

Chr	Position	SNP_ID	Gene	Residue Change	MAF_1000 Genomes	Reference allele	EADM02 (III:4)	EADQ01 (II:1)	EADS03 (II:3, AD)	EADX04 (III:3)	AD_AC	AD_AN	ctrl_AC	ctrl_AN	Fisher P	OR
chr19	45411941	rs429358	APOE	C130R	0.1506	C	T/C	T/C	T/T	T/C	80	332	61	736	1.12E-11	3.51
chr3	38167080	rs117916664	ACAA1	N299S	0.0038	T	T/C	T/C	C/C	T/C	17	324	15	736	9.85E-3	2.66
chr4	106158550	rs141975400	TET2	E1151*	0.0012	G	G/G	G/G	G/T	G/G	2	212	3	576	0.62	1.82
chr17	33550428	rs537835860	TBC1D3D	K25*	NA	T	T/T	T/T	T/A	T/T	1	182	7	736	1.00	0.58
chr11	48266736	rs7120775	OR4X2	Y27*	0.0028	C	C/C	C/C	C/G	C/C	57	320	NA	NA	1.00	NA
chrX	14027177	rs3747421	GEMIN8	E195V	0.0050	T	T/A	T/A	A/A	T/T	45	318	NA	NA	1.00	NA
chrX	32404572	rs72468638	DMD	K1510R	0.0014	T	T/C	T/C	C/C	T/T	4	336	NA	NA	1.00	NA
chr5	1240757	rs7447815	SLC6A18	Y319*	0.0006	C	C/G	G/G	G/G	C/G	110	332	NA	NA	1.00	NA
chrX	135426968	rs5930931	GPR112	P368H	0.0001	C	C/A	C/A	A/A	C/C	81	318	NA	NA	1.00	NA
chr19	43698682	-	PSG4	Y351*	NA	G	G/G	G/G	G/C	G/G	NA	NA	NA	NA	NA	NA
chr7	4304937	rs117504728	SDK1	T2188K	0.0096	C	C/A	C/C	C/A	C/A	7	310	39	736	0.03	0.41
chr15	40916632	rs141726041	CASC5	D1390E	0.0066	T	T/A	T/A	T/A	T/T	14	336	16	736	0.07	1.96
chr1	51826853	rs151081025	EPS15	N845S	0.0086	T	T/C	T/C	T/C	T/T	10	324	11	736	0.10	2.10
chr2	234201922	rs140671487	ATG16L1	A531V	0.0050	C	C/T	C/T	C/T	C/T	9	338	26	526	0.11	0.53
chr19	10736346	rs201831788	SLC44A2	G13R	0.0088	G	G/A	G/A	G/A	G/A	9	334	32	734	0.23	0.6
chr1	24840882	rs143770846	RCAN3	K7R	0.0014	A	A/G	A/G	A/G	A/A	4	214	7	736	0.28	1.98
chr16	21261289	-	ANKS4B	R134S	NA	G	G/C	G/G	G/C	G/G	1	212	0	366	0.37	5.20
chr12	56365381	rs2069413	CDK2	T256S	0.0044	C	C/G	C/G	C/G	C/C	11	322	19	736	0.43	1.34
chr3	64666931	rs140444427	ADAMTS9	R209C	0.0080	G	G/A	G/G	G/A	G/G	7	324	23	736	0.43	0.69
chr11	35250725	rs200125479	CD44	E649K	0.0002	G	G/A	G/G	G/A	G/A	1	212	1	576	0.47	2.73
chr1	214537946	rs200340171	PTPN14	P1115L	0.0032	G	G/A	G/G	G/A	G/A	6	338	14	526	0.49	0.66
chr3	49947940	-	MON1A	A428T	NA	C	C/T	C/C	C/T	C/T	3	312	0	160	0.55	NA
chr1	153651621	-	NPR1	R13S	NA	C	C/A	C/C	C/A	C/A	2	202	1	318	0.56	3.17
chr7	1588206	rs150440402	TMEM184A	V255I	0.0026	C	C/T	C/T	C/T	C/T	7	322	13	736	0.63	1.24
chr15	41148251	rs116845898	SPINT1	G427S	0.0050	G	G/A	G/A	G/A	G/A	5	318	16	736	0.64	0.72
chr3	39166625	rs148183642	TTC21A	V397M	0.0036	G	G/A	G/G	G/A	G/A	1	214	7	736	0.69	0.49
chr17	19687216	rs55730189	ULK2	G752R	0.0058	C	C/T	C/T	C/T	C/T	9	326	19	736	0.84	1.07

Chr	Position	SNP_ID	Gene	Residue Change	MAF_1000 Genomes	Reference allele	EADM02 (III:4)	EADQ01 (II:1)	EADS03 (II:3, AD)	EADX04 (III:3)	AD_AC	AD_AN	ctrl_AC	ctrl_AN	Fisher P	OR
chr17	21202191	rs33911218	MAP2K3	P11T	0.0002	C	C/A	C/A	C/A	C/A	168	330	160	320	0.88	1.04
chr12	1040408	rs370272002	RAD52	R55H	NA	C	C/T	C/C	C/T	C/C	1	212	0	160	1.00	2.28
chr17	10398298	rs140873918	MYH1	Q1806K	0.0004	G	G/T	G/T	G/T	G/T	1	210	2	576	1.00	1.37
chr16	28603585	rs55845129	SULT1A2	K258N	0.0016	T	T/A	T/T	T/A	T/T	2	212	8	736	1.00	0.87
chr3	37670789	rs147773336	ITGA9	R601C	0.0004	C	C/T	C/C	C/T	C/T	1	214	4	526	1.00	0.61
chr2	43452757	rs201963284	ZFP36L2	H62Q	0.0020	A	A/C	A/A	A/C	A/A	3	328	5	576	1.00	1.05
chr5	1815983	-	NDUFS6	G110C	NA	G	G/T	G/T	G/T	G/G	NA	NA	NA	NA	NA	NA
chr17	10551887	-	MYH3	N241S	NA	T	T/C	T/C	T/C	T/C	NA	NA	NA	NA	NA	NA
chr11	498548	-	RNH1	L289F	NA	G	G/A	G/A	G/A	G/G	NA	NA	NA	NA	NA	NA
chr14	23549329	-	ACIN1	E463D	NA	C	C/G	C/G	C/G	C/G	NA	NA	NA	NA	NA	NA
chr11	27016120	-	FIBIN	C16Y	NA	G	G/A	G/A	G/A	G/G	NA	NA	NA	NA	NA	NA
chr16	27454345	rs146177564	IL21R	R139C	0.0024	C	C/T	C/T	C/T	C/C	NA	NA	NA	NA	NA	NA
chr14	36004753	-	INSM2	H432L	NA	A	A/T	A/T	A/T	A/A	NA	NA	NA	NA	NA	NA
chr3	47883141	-	DHX30	A196T	NA	G	G/A	G/G	G/A	G/A	NA	NA	NA	NA	NA	NA
chr12	53897517	-	TARBP2	S116F	NA	C	C/T	C/T	C/T	C/C	NA	NA	NA	NA	NA	NA
chr14	57046739	-	C14orf101	V36A	NA	T	T/C	T/C	T/C	T/T	NA	NA	NA	NA	NA	NA
chr16	58757654	rs138952206	GOT2	R81H	0.0002	C	C/T	C/C	C/T	C/T	NA	NA	NA	NA	NA	NA
chr15	59499363	-	LDHAL6B	I75T	NA	T	T/C	T/C	T/C	T/T	NA	NA	NA	NA	NA	NA
chr20	60883146	rs373828612	ADRM1	R309H	NA	G	G/A	G/G	G/A	G/A	NA	NA	NA	NA	NA	NA
chr14	62187265	-	HIF1A	L67F	NA	G	G/T	G/T	G/T	G/G	NA	NA	NA	NA	NA	NA
chr16	68267770	rs78705766	ESRP2	D153N	0.0002	C	C/T	C/C	C/T	C/T	NA	NA	NA	NA	NA	NA
chr16	69875980	rs184547498	WWP2	R178W	0.0002	C	C/T	C/C	C/T	C/T	NA	NA	NA	NA	NA	NA
chr9	79634858	-	FOXB2	M96I	NA	G	G/T	G/G	G/T	G/G	NA	NA	NA	NA	NA	NA
chr11	102589280	-	MMP8	H217Y	NA	G	G/A	G/G	G/A	G/G	NA	NA	NA	NA	NA	NA
chr13	103446154	-	KDELC1	P131S	NA	G	G/A	G/G	G/A	G/G	NA	NA	NA	NA	NA	NA
chr2	107423238	-	ST6GAL2	N496D	NA	T	T/C	T/T	T/C	T/T	NA	NA	NA	NA	NA	NA
chr11	129753091	-	NFRKB	D276G	NA	T	T/C	T/C	T/C	T/T	NA	NA	NA	NA	NA	NA
chr9	140289770	rs374664490	EXD3	E14K	NA	C	C/T	C/C	C/T	C/T	NA	NA	NA	NA	NA	NA
chr6	145114993	rs116739902	UTRN	P2982S	0.0012	C	C/T	C/T	C/T	C/C	NA	NA	NA	NA	NA	NA

Chr	Position	SNP_ID	Gene	Residue Change	MAF_1000 Genomes	Reference allele	EADM02 (III:4)	EADQ01 (II:1)	EADS03 (II:3, AD)	EADX04 (III:3)	AD_AC	AD_AN	ctrl_AC	ctrl_AN	Fisher P	OR
chr1	147380272	-	GJA8	V64I	NA	G	G/A	G/G	G/A	G/A	NA	NA	NA	NA	NA	NA
chr7	150644474	rs373394254	KCNH2	R1032W	0.0004	G	G/A	G/G	G/A	G/G	NA	NA	NA	NA	NA	NA
chr1	161993059	-	OLFML2B	N54K	NA	G	G/T	G/G	G/T	G/T	NA	NA	NA	NA	NA	NA

Chr, chromosome; Position, physical position of the variant; SNP_ID, rsID in dbSNP (<https://www.ncbi.nlm.nih.gov/snp/>); MAF_1000Genomes, minor allele frequency in the dataset of the 1000 Genomes Project^{22,23}; Reference allele, allele of reference genome hg19 (GRCh37: https://grch37.ensembl.org/Homo_sapiens); AD_AC, allele count of AD cases; AD_AN, allele number of AD cases; ctrl_AC, allele count of the controls; ctrl_AN, allele number of the controls; Fisher P, Fisher exact P-value; OR, odds ratio. 107 patients with early onset familial AD (EOFAD) enrolled from South China (Yunnan, Hunan, and Sichuan provinces)¹⁶ and 62 EOFAD cases collected from North China (Beijing, Hebei, and Shandong provinces)²¹ were considered as the AD cases. The control (ctl) sample referred to the population control described in our previous study¹⁶, which contained 386 pooled Han Chinese individuals from different sources.

Table S3.

KEGG pathway, GO CC (cellular component) and GO BP (biological processes) analyses of dysregulated genes in the HM and U251-APP cells in ACAA1 p.N299S group compared with ACAA1 WT group

Cell Type	Type	ID	Description	<i>P</i> -value ^a	<i>P</i> _{adjust} ^b	FDR q-value ^c
HM	KEGG	hsa04142	Lysosome	2.50E-04	9.06E-03	8.06E-03
HM	KEGG	hsa04218	Cellular senescence	5.58E-04	1.27E-02	1.13E-02
U251-APP	KEGG	hsa05010	Alzheimer's Disease	2.78E-20	3.05E-18	2.26E-18
U251-APP	KEGG	hsa04142	Lysosome	6.96E-06	1.64E-04	1.21E-04
U251-APP	KEGG	hsa04722	Neurotrophin signaling pathway	1.78E-03	1.41E-02	1.04E-02
U251-APP	KEGG	hsa04218	Cellular senescence	4.83E-06	1.32E-04	9.82E-05
U251-APP	KEGG	hsa04979	Cholesterol metabolism	5.99E-03	3.34E-02	2.48E-02
U251-APP	GO-CC	GO:0043202	Lysosomal lumen	1.64E-06	2.49E-05	1.82E-05
U251-APP	GO-CC	GO:0030426	Growth cone	4.10E-06	5.30E-05	3.88E-05
U251-APP	GO-CC	GO:0099572	Postsynaptic specialization	9.44E-05	8.24E-04	6.03E-04
U251-APP	GO-CC	GO:0098984	Neuron to neuron synapse	1.69E-05	1.74E-04	1.28E-04
U251-APP	GO-CC	GO:0048786	Presynaptic active zone	1.09E-03	7.41E-03	5.43E-03
U251-APP	GO-CC	GO:0150034	Distal axon	2.31E-03	1.39E-02	1.02E-02
HM	GO-CC	GO:0014069	Postsynaptic density	1.74E-08	4.35E-07	3.39E-07
HM	GO-CC	GO:0098984	Neuron to neuron synapse	9.25E-08	2.04E-06	1.59E-06
HM	GO-CC	GO:0043202	Lysosomal lumen	3.67E-07	7.35E-06	5.73E-06
HM	GO-CC	GO:0005765	Lysosomal membrane	8.58E-06	1.45E-04	1.13E-04
HM	GO-CC	GO:0097386	Glial cell projection	1.03E-04	1.29E-03	1.00E-03
HM	GO-CC	GO:0150034	Distal axon	2.66E-04	2.91E-03	2.27E-03
HM	GO-CC	GO:0098685	Schaffer collateral - CA1 synapse	2.06E-03	1.65E-02	1.29E-02
HM	GO-CC	GO:0043197	Dendritic spine	3.34E-03	2.47E-02	1.92E-02
HM	GO-CC	GO:0044309)	Neuron spine	4.23E-03	3.05E-02	2.38E-02
HM	GO-CC	GO:0048786	Presynaptic active zone	4.59E-03	3.26E-02	2.54E-02
U251-APP	GO-BP	GO:0007041	Lysosomal transport	6.62E-10	5.34E-08	4.57E-08
U251-APP	GO-BP	GO:0008089	Anterograde axonal transport	1.00E-03	1.38E-02	1.18E-02
U251-APP	GO-BP	GO:0098930	Axonal transport	3.03E-03	3.37E-02	2.89E-02

Cell Type	Type	ID	Description	<i>P</i> -value ^a	<i>P</i> _{adjust} ^b	FDR q-value ^c
U251-APP	GO-BP	GO:0006622	Protein targeting to lysosome	1.74E-03	2.16E-02	1.85E-02
U251-APP	GO-BP	GO:0032226	Positive regulation of synaptic transmission, dopaminergic	2.17E-04	3.88E-03	3.32E-03
U251-APP	GO-BP	GO:0150003	Regulation of spontaneous synaptic transmission	2.18E-04	3.88E-03	3.32E-03
U251-APP	GO-BP	GO:1900272	Negative regulation of long-term synaptic potentiation	9.17E-04	1.28E-02	1.09E-02
U251-APP	GO-BP	GO:0032225	Regulation of synaptic transmission, dopaminergic	3.91E-03	4.12E-02	3.53E-02
U251-APP	GO-BP	GO:1900453	Negative regulation of long-term synaptic depression	2.04E-03	2.42E-02	2.07E-02
U251-APP	GO-BP	GO:0031914	Negative regulation of synaptic plasticity	1.99E-02	1.35E-01	1.15E-01
U251-APP	GO-BP	GO:1990090	Cellular response to nerve growth factor stimulus	4.11E-04	6.65E-03	5.70E-03
U251-APP	GO-BP	GO:1990089	Response to nerve growth factor	4.55E-04	7.21E-03	6.17E-03
U251-APP	GO-BP	GO:0090647	Modulation of age-related behavioral decline	7.65E-05	1.60E-03	1.37E-03
U251-APP	GO-BP	GO:1901216	Positive regulation of neuron death	4.01E-05	9.41E-04	8.06E-04
U251-APP	GO-BP	GO:0008654	Phospholipid biosynthetic process	1.05E-05	2.92E-04	2.50E-04
U251-APP	GO-BP	GO:0044242	Cellular lipid catabolic process	6.80E-04	9.81E-03	8.40E-03
U251-APP	GO-BP	GO:0006643	Membrane lipid metabolic process	3.71E-03	3.95E-02	3.38E-02
U251-APP	GO-BP	GO:0046466	Membrane lipid catabolic process	4.34E-03	4.45E-02	3.81E-02
U251-APP	GO-BP	GO:0034440	Lipid oxidation	6.88E-03	6.24E-02	5.34E-02
U251-APP	GO-BP	GO:0006635	Fatty acid beta-oxidation	1.59E-04	3.00E-03	2.57E-03
U251-APP	GO-BP	GO:0019395	Fatty acid oxidation	4.70E-03	4.77E-02	4.08E-02
HM	GO-BP	GO:0050808	Synapse organization	3.09E-08	2.41E-06	2.03E-06
HM	GO-BP	GO:0051963	Regulation of synapse assembly	1.77E-05	7.09E-04	5.97E-04
HM	GO-BP	GO:0050803	Regulation of synapse structure or activity	2.28E-05	8.53E-04	7.19E-04
HM	GO-BP	GO:0048167	Regulation of synaptic plasticity	3.07E-05	1.09E-03	9.20E-04
HM	GO-BP	GO:0050807	Regulation of synapse organization	3.34E-05	1.18E-03	9.94E-04
HM	GO-BP	GO:0035418	Protein localization to synapse	3.51E-05	1.22E-03	1.03E-03
HM	GO-BP	GO:0007416	Synapse assembly	6.71E-05	2.02E-03	1.70E-03
HM	GO-BP	GO:1902473	Regulation of protein localization to synapse	7.20E-05	2.11E-03	1.77E-03
HM	GO-BP	GO:0050804	Modulation of chemical synaptic transmission	8.86E-05	2.51E-03	2.11E-03
HM	GO-BP	GO:0051965	Positive regulation of synapse assembly	9.40E-05	2.63E-03	2.22E-03
HM	GO-BP	GO:0099177	Regulation of trans-synaptic signaling	9.75E-05	2.71E-03	2.28E-03
HM	GO-BP	GO:1903539	Protein localization to postsynaptic membrane	1.64E-04	4.08E-03	3.44E-03

Cell Type	Type	ID	Description	<i>P</i> -value ^a	<i>P</i> _{adjust} ^b	FDR q-value ^c
HM	GO-BP	GO:1905606	Regulation of presynapse assembly	3.01E-04	6.66E-03	5.61E-03
HM	GO-BP	GO:0099174	Regulation of presynapse organization	4.56E-04	9.43E-03	7.95E-03
HM	GO-BP	GO:0099054	Presynapse assembly	5.25E-04	1.03E-02	8.72E-03
HM	GO-BP	GO:0098969	Neurotransmitter receptor transport to postsynaptic membrane	1.01E-03	1.72E-02	1.45E-02
HM	GO-BP	GO:0048169	Regulation of long-term neuronal synaptic plasticity	1.27E-03	2.04E-02	1.72E-02
HM	GO-BP	GO:0099172	Presynapse organization	1.28E-03	2.05E-02	1.72E-02
HM	GO-BP	GO:1902474	Positive regulation of protein localization to synapse	1.40E-03	2.20E-02	1.85E-02
HM	GO-BP	GO:0099173	Postsynapse organization	1.57E-03	2.44E-02	2.05E-02
HM	GO-BP	GO:1903540	Establishment of protein localization to postsynaptic membrane	1.68E-03	2.56E-02	2.15E-02
HM	GO-BP	GO:0007411	Axon guidance	4.16E-10	4.07E-08	3.43E-08
HM	GO-BP	GO:0007409	Axonogenesis	5.23E-10	5.06E-08	4.26E-08
HM	GO-BP	GO:0050770	Regulation of axonogenesis	1.72E-08	1.38E-06	1.16E-06
HM	GO-BP	GO:0050771	Negative regulation of axonogenesis	1.37E-05	5.72E-04	4.82E-04
HM	GO-BP	GO:0030516	Regulation of axon extension	1.87E-05	7.41E-04	6.24E-04
HM	GO-BP	GO:0050772	Positive regulation of axonogenesis	9.81E-05	2.71E-03	2.28E-03
HM	GO-BP	GO:0048675	Axon extension	1.55E-04	3.99E-03	3.36E-03
HM	GO-BP	GO:0030517	Negative regulation of axon extension	8.48E-04	1.52E-02	1.28E-02
HM	GO-BP	GO:0036515	Serotonergic neuron axon guidance	1.29E-03	2.05E-02	1.72E-02
HM	GO-BP	GO:1902667	Regulation of axon guidance	2.03E-03	2.96E-02	2.50E-02
HM	GO-BP	GO:0019896	Axonal transport of mitochondrion	2.96E-03	3.91E-02	3.30E-02
HM	GO-BP	GO:0048841	Regulation of axon extension involved in axon guidance	3.12E-03	4.07E-02	3.43E-02
HM	GO-BP	GO:0008366	Axon ensheathment	3.16E-03	4.10E-02	3.45E-02
HM	GO-BP	GO:0071398	Cellular response to fatty acid	9.65E-04	1.68E-02	1.41E-02
HM	GO-BP	GO:0070542	Response to fatty acid	1.50E-03	2.34E-02	1.97E-02
HM	GO-BP	GO:0007611	Learning or memory	8.57E-05	2.44E-03	2.05E-03
HM	GO-BP	GO:0007613	Memory	2.11E-03	3.06E-02	2.58E-02
HM	GO-BP	GO:0097485	Neuron projection guidance	2.25E-10	2.25E-08	1.90E-08
HM	GO-BP	GO:0010977	Negative regulation of neuron projection development	9.41E-07	5.54E-05	4.67E-05
HM	GO-BP	GO:0045665	Negative regulation of neuron differentiation	1.51E-06	8.50E-05	7.16E-05
HM	GO-BP	GO:0010976	Positive regulation of neuron projection development	1.97E-06	1.07E-04	9.02E-05

Cell Type	Type	ID	Description	<i>P</i> -value ^a	<i>P</i> _{adjust} ^b	FDR q-value ^c
HM	GO-BP	GO:0045666	Positive regulation of neuron differentiation	3.12E-06	1.56E-04	1.32E-04
HM	GO-BP	GO:1990138	Neuron projection extension	2.40E-05	8.83E-04	7.44E-04
HM	GO-BP	GO:0021954	Central nervous system neuron development	6.59E-05	2.00E-03	1.69E-03
HM	GO-BP	GO:0051402	Neuron apoptotic process	4.66E-04	9.60E-03	8.09E-03
HM	GO-BP	GO:0043524	Negative regulation of neuron apoptotic process	5.79E-04	1.13E-02	9.53E-03
HM	GO-BP	GO:0048169	Regulation of long-term neuronal synaptic plasticity	1.27E-03	2.04E-02	1.72E-02
HM	GO-BP	GO:0036515	Serotonergic neuron axon guidance	1.29E-03	2.05E-02	1.72E-02
HM	GO-BP	GO:0021953	Central nervous system neuron differentiation	1.34E-03	2.12E-02	1.78E-02
HM	GO-BP	GO:0043523	Regulation of neuron apoptotic process	1.58E-03	2.45E-02	2.06E-02
HM	GO-BP	GO:0070997	Neuron death	2.06E-03	3.00E-02	2.53E-02
HM	GO-BP	GO:0001764	Neuron migration	2.50E-03	3.51E-02	2.95E-02
HM	GO-BP	GO:0007272	Ensheathment of neurons	3.16E-03	4.10E-02	3.45E-02

KEGG, Kyoto Encyclopedia of Genes and Genomes; GO-CC, gene ontology-cellular component; GO-BP, gene ontology-biological processes; FDR: false discovery rate.

^a *P*-value of the enrichment analysis calculated by hypergeometric test

^b *P*_{adjust}, the BH-adjusted *P*-value, was calculated by adjusted *P*-value with Benjamini-Hochberg (BH) method

^c FDR q-value was calculated by adjusted *P*-value with an optimized false discovery rate (FDR) approach

Table S4.**Primary and secondary antibodies and chemicals used in this study**

Antibodies	Source	Catalog no.	Western blot	IF	IHC
<i>Primary antibody</i>					
Rabbit monoclonal anti-GluR1 (phospho S381)	Abcam	ab109464	1:1000	-	-
Rabbit polyclonal anti-GluR1	Elabscience	E-AB-31551	1:1000	-	-
Rabbit polyclonal anti-GRIN2B	Elabscience	E-AB-15807	1:1000	-	-
Rabbit polyclonal anti-LAMP1	Abcam	ab24170	1:1000	-	-
Rabbit polyclonal anti-CTSB	Affinity Bioscience	DF6149	1:1000	-	-
Rabbit monoclonal ACAA1	Cell Signaling Technology	12210	1:1000	-	-
Rabbit polyclonal anti-CTSD	Cell Signaling Technology	DF6486	1:1000	-	-
Rabbit polyclonal anti-PSD95	Abcam	ab18258	1:1000	-	-
Rabbit polyclonal anti-TFEB	Cell Signaling Technology	4240	1:1000	-	-
Rabbit monoclonal anti-NeuN	Abcam	ab177487	1:1000	1:500	-
Mouse monoclonal anti-IBA1	Millipore	MABN92	-	1:300	-
Mouse monoclonal anti-Flag-Tag	EnoGene	E12-001	1:10000	-	-
Rabbit monoclonal anti-LAMP2A	Abcam	ab125068	1:1000	-	-
Mouse monoclonal anti-Synaptophysin	Millipore	MAB5258-50UG	1:10000	-	-
Mouse monoclonal anti-GFP	EnoGene	E12-009	1:1000	-	-
Chicken polyclonal anti-GFP	Abcam	ab13970	-	500	-
Rabbit polyclonal anti-MAP1LC3/LC3	Proteintech	14600-1-AP	1:1000	-	-
Rabbit polyclonal anti-SQSTM1	Elabscience	EAP3350	1:1000	-	-
Rabbit monoclonal anti anti-PEN2	Cell Signaling Technology	8598	1:1000	-	-
Rabbit monoclonal anti-PSEN1	Cell Signaling Technology	5643	1:1000	-	-
Rabbit monoclonal anti-PSEN2	Cell Signaling Technology	9979	1:1000	-	-
Rabbit monoclonal anti-BACE1	Cell Signaling Technology	5606	1:1000	-	-
Mouse anti- β -amyloid,17–24(4G8)	BioLegend	800701	-	1:500	1:500
Mouse monoclonal anti- β -tubulin	EnoGene	E1C601	1:10000	-	-
Mouse monoclonal anti-GAPDH	Proteintech	60004-1-Ig	1:10000	-	-
Mouse monoclonal anti-ACTB	Beijing Zhong Shan-Golden Bridge Biological Technology CO., LTD	TA-09	1:10000	-	-
<i>Secondary antibody</i>					
Peroxidase-conjugated anti-rabbit antibody	KPL	474-1516	1:10000	-	-

Peroxidase-conjugated anti-mouse antibody	KPL	474-1806	1:10000	-	-
Alexa Fluor® 594-conjugated anti-rabbit IgG	Invitrogen	A21207	-	1:500	-
Alexa Fluor® 488-conjugated anti-chicken IgG	Invitrogen	A11039	-	1:500	-
Alexa Fluor® 555 anti-mouse IgG	Invitrogen	A31570	-	1:500	-
HRP-conjugated goat anti-mouse antibody	Servicebio	GB23301	-	-	1:200
Chemicals					
	Source	Catalog no.	-	-	-
4', 6-diamidino-2-phenylindole (DAPI)	Roche	10236276001	-	-	-
Bafilomycin A1 (BAFA1)	InvivoGen	tlrl-baf	-	-	-
NH4CL	Sigma	A9434	-	-	-
Pentobarbital	Sigma	P3761	-	-	-

IF - immunofluorescence; IHC - Immunohistochemistry

Reference

- 1 Zhang, D. F. *et al.* CFH variants affect structural and functional brain changes and genetic risk of Alzheimer's disease. *Neuropsychopharmacol* **41**, 1034-1045 (2016).
- 2 Xiang, Q. *et al.* Rare genetic variants of the Transthyretin gene are associated with Alzheimer's disease in Han Chinese. *Mol Neurobiol* **54**, 5192-5200 (2017).
- 3 Kumar, S., Stecher, G. & Tamura, K. MEGA7: molecular evolutionary genetics analysis version 7.0 for bigger datasets. *Mol Biol Evol* **33**, 1870-1874 (2016).
- 4 Xu, M. *et al.* A systematic integrated analysis of brain expression profiles reveals YAP1 and other prioritized hub genes as important upstream regulators in Alzheimer's disease. *Alzheimers Dement* **14**, 215-229 (2018).
- 5 Bolger, A. M., Lohse, M. & Usadel, B. Trimmomatic: a flexible trimmer for Illumina sequence data. *Bioinformatics* **30**, 2114-2120 (2014).
- 6 Dobin, A. *et al.* STAR: ultrafast universal RNA-seq aligner. *Bioinformatics* **29**, 15-21 (2013).
- 7 Liao, Y., Smyth, G. K. & Shi, W. The Subread aligner: fast, accurate and scalable read mapping by seed-and-vote. *Nucleic Acids Res* **41**, e108 (2013).
- 8 Love, M. I., Huber, W. & Anders, S. Moderated estimation of fold change and dispersion for RNA-seq data with DESeq2. *Genome Biol* **15**, 550 (2014).
- 9 The Gene Ontology, C. The Gene Ontology Resource: 20 years and still GOing strong. *Nucleic Acids Res* **47**, D330-D338 (2019).
- 10 Kanehisa, M., Furumichi, M., Tanabe, M., Sato, Y. & Morishima, K. KEGG: new perspectives on genomes, pathways, diseases and drugs. *Nucleic Acids Res* **45**, D353-D361 (2017).
- 11 Yu, G., Wang, L. G., Han, Y. & He, Q. Y. clusterProfiler: an R package for comparing biological themes among gene clusters. *OMICS* **16**, 284-287 (2012).
- 12 Subramanian, A. *et al.* Gene set enrichment analysis: a knowledge-based approach for interpreting genome-wide expression profiles. *Proc Natl Acad Sci U S A* **102**, 15545-15550 (2005).
- 13 Luo, R. *et al.* Activation of PPARA-mediated autophagy reduces Alzheimer disease-like pathology and cognitive decline in a murine model. *Autophagy* **16**, 52-69 (2020).
- 14 Su, L. Y. *et al.* Atg5- and Atg7-dependent autophagy in dopaminergic neurons regulates cellular and behavioral responses to morphine. *Autophagy* **13**, 1496-1511 (2017).
- 15 Sheng, N., Shi, Y. S. & Nicoll, R. A. Amino-terminal domains of kainate receptors determine the differential dependence on Neto auxiliary subunits for trafficking. *Proc Natl Acad Sci U S A* **114**, 1159-1164 (2017).
- 16 Zhang, D. F. *et al.* Complement C7 is a novel risk gene for Alzheimer's disease in Han Chinese. *Natl Sci Rev* **6**, 257-274 (2019).
- 17 Fu, A. K. Y. *et al.* IL-33 ameliorates Alzheimer's disease-like pathology and cognitive decline. *P Natl Acad Sci USA* **113**, E2705-E2713 (2016).
- 18 Alves, S. *et al.* Interleukin-2 improves amyloid pathology, synaptic failure and memory in Alzheimer's disease mice. *Brain* **140**, 826-842 (2017).
- 19 Martinez Hernandez, A. *et al.* The diphenylpyrazole compound anle138b blocks Abeta channels and rescues disease phenotypes in a mouse model for amyloid pathology. *EMBO Mol Med* **10**, 32-47 (2018).
- 20 Krauthausen, M. *et al.* CXCR3 promotes plaque formation and behavioral deficits in an

- Alzheimer's disease model. *J Clin Invest* **125**, 365-378 (2015).
- 21 Wang, G. *et al.* Mutation and association analyses of dementia-causal genes in Han Chinese patients with early-onset and familial Alzheimer's disease. *J Psychiatr Res* **113**, 141-147 (2019).
 - 22 Sudmant, P. H. *et al.* An integrated map of structural variation in 2,504 human genomes. *Nature* **526**, 75-81 (2015).
 - 23 Genomes Project, C. *et al.* A global reference for human genetic variation. *Nature* **526**, 68-74 (2015).
 - 24 Kumar, P., Henikoff, S. & Ng, P. C. Predicting the effects of coding non-synonymous variants on protein function using the SIFT algorithm. *Nat Protoc* **4**, 1073-1081 (2009).
 - 25 Adzhubei, I. A. *et al.* A method and server for predicting damaging missense mutations. *Nat Methods* **7**, 248-249 (2010).
 - 26 Adzhubei, I., Jordan, D. M. & Sunyaev, S. R. Predicting functional effect of human missense mutations using PolyPhen-2. *Curr Protoc Hum Genet* **Chapter 7**, Unit7 20 (2013).
 - 27 Chun, S. & Fay, J. C. Identification of deleterious mutations within three human genomes. *Genome Res* **19**, 1553-1561 (2009).
 - 28 Schwarz, J. M., Cooper, D. N., Schuelke, M. & Seelow, D. MutationTaster2: mutation prediction for the deep-sequencing age. *Nat Methods* **11**, 361-362 (2014).